Modeling of the Space Rider flight dynamics during the terminal descent phase

Modeling of the Space Rider flight dynamics during the terminal descent phase

Author:
Matthis de Lange (1009253)

Supervisors:
dr. ir. Roland Tóth
ir. Chris Verhoek

External supervisor:
dr. Valentin Preda (ESA)

Eindhoven University of Technology, 2021

Department of Electrical Engineering

Abstract

The European Space Agency (ESA) is developing a module, named the Space Rider (SR). With the SR it is possible to do research in the earths low orbit. The SR can return to earth and is capable of landing at a predefined position by means of a guided parafoil. This report discusses, which dynamical effects are relevant to construct a model, describing the flight dynamics of the SR during its guided parafoil descend. First the already existing models, which are found in the literature, are discussed. A 6 degrees of freedom (DoF) and a 12 DoF model is presented. THe models are simulated in Simulink. The results are analyses and compared with simulation results found in the literature for an already existing model. The models are linearized and the flight dynamics of the linearizations are analyzed. It can be concluded that the gravity, aerodynamics and apparent mass are all relevant to the flight dynamics during the descent of the SR. The 6 DoF models shows the overall flight behavior needed for position, velocity and heading control. The 12 DOF model give additional dynamics, which are insightful in the presence of wind disturbances or during the landing.

List of Symbols

Table 1: Model parameters

Symbol	Definition	Unit
g	Gravity constant	ms^{-2}
ρ	Air pressure	kg/m^3
$I_{\mathrm{p}}^{\mathrm{p}}$	Parafoil inertia matrix	kgm^2
m_{p}	Parafoil mass	kg
b_{p}	Parafoil wingspan	m
c_{p}	Parafoil chord	m
t_{p}	Parafoil thickness	m
S_{p}	Parafoil reference area	m^2
μ	Parafoil rigging angle	rad
$m_{\mathrm{am}}^{\mathrm{p}}$	Parafoil apparent mass matrix	kg
$I_{\mathrm{am}}^{\mathrm{p}}$	Parafoil apparent inertia matrix	kgm^2
$I_{\mathrm{l}}^{\mathrm{l}}$	Load inertia matrix	kgm^2
m_{l}	Load mass	kg
S_{l}	Load reference area	m^2
$r_{\mathrm{p}}^{\mathrm{c}}$	Parafoil mass position vector	m
$r_{\mathrm{am}}^{\mathrm{c}}$	Apparent mass position vector	m
$r_{\mathrm{l}}^{\mathrm{c}}$	Load mass position vector	m
C_{Fp}	Parafoil aerodynamic force coefficients	$-$
C_{Mp}	Parafoil aerodynamic moment coefficients	$-$
C_{Fl}	Load aerodynamic force coefficients	$-$
C_{Ml}	Load aerodynamic moment coefficients	$-$
$K_{\mathrm{t},\vec{r}}$	Spring coefficient matrix	N/m
$K_{\mathrm{t},\vec{\eta}}$	Torsion spring coefficient matrix	N/rad
$D_{\mathrm{t},\vec{r}}$	Damping coefficient matrix	Ns/m
$D_{\mathrm{t},\vec{\eta}}$	Torsion damping coefficient matrix	Ns/rad

Contents

1 Introduction

Research in low earth orbit gives opportunities for experiments and exploration of technology, which is not possible in a planet environment, because it is dominated by gravity. To overcome the effect of gravity to do microgravity research, multiple methods are currently used. Like a vacuum chamber, in which a free fall can be reached, an airplane in parabolic flight or by launching a rocket within the earths atmosphere. The approaches have limitations on the experiment length up to several minutes. Therefore, ESA is currently developing a module, the Space Rider (SR), that can do research in low orbit. The SR is launched in low orbit and can stay there for multiple months to perform microgravity research. Other possible tasks could be validation and demonstration of robotic exploration, earth observation and telecommunication. Even satellite inspection is a possibility [1].

One of the objectives of the project is the re-usability of the SR. Therefore, the SR should return to the earth, such that it is undamaged and retrievable. A strategy is developed for the decent of the SR. First, the SR re-enters the atmosphere at a high velocity. As following, A drogue parachute is used to decelerate the SR to a velocity and altitude at which the guided parafoil can be deployed. With the guided parafoil, the SR ca steer and navigate to the landing point, where it eventually lands gently. This last part, which is the terminal guidance phase, is full of challenges. The control of the SR is handled by the Guidance, Navigation and Control system (GNC) and should be able to guide the SR to a precision landing in the presence of wind disturbances and ensure a soft landing. A soft landing means an impact with bounded velocity.

One way to quantify the performance of the developed GNC solution is by performing a Monte-Carlo simulation for different wind disturbances and creating a normal distribution around the landing position and the desired impact velocity. This can provide sufficient verification of the landing precision of the GNC. To support the development of such a simulation environment a model is needed that captures the relevant descending dynamics of the SR with the parafoil [2]. The developed GNC solution can be improved with the simulation environment. This report answers the question: Which dynamic effects acting on the SR during the terminal guidance phase should be considered, to describe the flight dynamics of the Space Rider w.r.t. the desired landing precision and landing constraints of the GNC system?

The Space Rider during the terminal descent phase is connected to the parafoil with tension lines as shown in Figure 1. The Space Rider steers itself by deflecting the parafoils trailing edge, eventually very similar as an airplane would be steered. The steering lines, which are not the same as the tension lines, connect the trailing edge of the parafoil and the SR. They are controlled by the GNC system. The SR with the guided parafoil falls in the category of precision aerial delivery systems (PADS) and can be modeled accordingly.

Figure 1: The Space Rider guided by a parafoil

Yakimenko [3] gives an overview of some proposed models to capture the flight dynamics of a PADS. As low fidelity model a 3 DoF model is used, assuming a point mass moving with a velocity in three directions. The complexity is increased with a 6 DoF model, where the whole system is assumed to be one rigid body. By including some relative DoF between the parafoil and the load a 7-9 DoF model can be created. A 12 DoF model is obtained when the load can move in all six directions relative to the parafoil. The models included aerodynamics, apparent mass and gravity as dynamc effects.

The report structure is as following. First, a literature overview is given. The existing models, which describe the flight dynamics of a PADS are presented, in terms of the included dynamic effects. Next a 6 DoF mathematical model is proposed for a PADS, which is extended to a 12 DoF model. In the models, the aerodynamic effect, apparent mass effect and the gravity will be considered. As following the implementation of these mathematical models in SIMULINK is shown and the flight dynamics are analyses through simulation of the model implementation. Especially, the contribution of the apparent mass to the flight dynamics and the differences in the flight dynamics between the 6 DoF and the 12 DoF models are analyzed. With the simulation results, the model is linearized in multiple operation points. The dynamic flight behavior of the linear models gives an overview of flight dynamics of the overall model and also gives an inside in the non-linearity of the overall model. This gives an insight to improve the GNC solution. Lastly, some notes are given on the presented work, together with future recommendations and a conclusion is made. w.r.t. the research question.

2 Literature review

In the literature a lot of different models, representing the flight dynamics of a PADS, are available. The presented models have varying complexity from 3-4 DoF models, 6 DoF models, 7-9 DoF models and a 12 DoF model. Furthermore, the models can be characterized by the included dynamics effects and how these dynamics are included. Sec. 2.1 describes the complexity order of the models and the included dynamc effects. Additional literature of the dynamic effects is discussed in Sec. 2.2 and 2.3. Also simulation parameters simulation results and experimental results are found in the literature and are discussed in Sec. 2.4.

2.1 Existing models and complexity

For each model complexity the included dynamic effects are discussed. the models are presented in order of complexity. The 3 DoF models are described by Yakimenko [4], Bonaccorsi [5] and Rademacher [6]. The model consists of a point mass, which can move in the x-y-z direction, with a velocity vector. The acting forces on the system are the gravity and aerodynamic lift and drag. The aerodynamics are modeled with a constant trim coefficient, which can be altered for the control deflections. With the control deflections the system can be decelerated and steered. A delay is used to approximate the repose time of the system to a control input. The output of the system are the position and velocity and the inputs are the control deflections. The wind is embedded as the disturbance. Yakimenko extends the model in [4] to a 4 DoF model by including a yawing rate in the model.

The model complexity is increased with the 6 DoF model, described by Figueroa-González [2], Yakimenko [3], [4], Bonaccorsi [5], Ward [7], and Mazouz [8]. The PADS is represented as one rigid body with a single mass and inertia. The model can move along the axis of a Cartesian coordinate system, but also rotate with the Euler angles. The model therefore considers the velocity vector but also the angular velocity. In the 6 DoF models the following dynamic effects are included. The gravity, still works the same as in the 4-3 DoF models. The aerodynamics, consisting of a drag, lift and side force as well as three aerodynamic moments. The aerodynamic coefficients are used to express the aerodynamic force and moment. These coefficients can be described with a linear model in an operation range as used by Yakimenko [3], [4], Bonaccorsi [5] and Mazouz [8] or with a mix of a look-up table and a linear model as is used by Figueroa-González [2]. In a 6 DoF model the apparent mass can be included. The apparent mass describes additional pressure forces on the body. Figueroa-González [2] argues that the effect is not significant for their application. They say it is only relevant for application with loading more than 5 $[Kg/m^2]$. Yakimenko [4], Bonaccorsi [5] and Mazouz [8] argue it is important for their application. They implement the apparent mass effect, with the momentum and angular momentum of the apparent mass being decoupled in a center of apparent mass. Yakimenko [3] also implements the effect in a version where the momentum and angular momentum of the apparent mass are not decoupled. The output of the model describes the position and orientation of rigid body with its velocity and angular rate. The input of the model are the control deflections and the wind is a disturbance.

The system derived by Ward [9] is considered a 6 DoF model. Even though the paper considers the parafoil and the load as separate rigid body, it also uses rigid connections to connect both bodies. These rigid lines can be controlled to vary the center of mass (CoM) of the system steer the direction of the system. The type aerodynamic model is the same as used by Yakimenko [4]. The apparent mass is considered, but the implementation manner remains unclear.

A 7-9 DoF model includes relative degrees to freedom between the parafoil and the load. Yakimenko [4] shows three models for 7-9 DoF. The aerodynamic and gravity are separated in a set of dynamic effects for the load and for the parafoil. Each degree of freedom represents an extra rotation the load can make, in an attachment point, w.r.t. the parafoil. The expressions for the aerodynamics of the load and parafoil are similar to the expressions used in the 6 DoF model. The apparent mass is considered in decoupled form.

Redelinghuys [10], Sleger [11], Yakimenko [3] and Zhu [12] all present an 8 DoF model. Zhu [12] allows a relative pitch and yaw angle between the load and the parafoil. The relative motion is constraint with tension forces. A torsional spring-damper system is used. To model the aerodynamics, the parafoil is divided in multiple panels and the aerodynamic drag and lift are modeled per panel. The aerodynamic moment is derived as a result of the aerodynamic force. The load is only influenced by a drag component. A linear model is used to determine the aerodynamic coefficients and a coupled apparent mass effect is considered. The 8 DoF model developed by [11] considers the same relative pitch and yaw angles as additional degrees of freedom. The same approach is used to constrain the relative angles, with tension forces. The aerodynamics are considered the same as used by Yakimenko [4]. The apparent mass effect is considered in decoupled form. Yakimenko [3] develops a general model structure for an 8 DoF model, but does not show how specific components can be modeled.

A different type of model is introduced by Redelinghuys [10]. The added DoF are still a relative pitch and yaw angle. Instead of defining the model along the classical Newtonian formulations, the model presented is based on the Hamiltonian approach. A non-linear restoring moment is formulated on the relative yaw angle. The paper considers the combination of a parafoil with an unmanned air vehicles (UAV). Therefore, a full aerodynamic expression is used for both the parafoil and the load. This includes a drag, lift and side force and all three aerodynamic moments. The coefficients for the parafoil are calculated with Computational Fluid Dynamics (CFD) and a fit was determined on top of the lookup table. This gives a linearization in a moving operation point. The aerodynamic coefficients of the UAV are constant and the apparent mass is not included.

A 12 DoF model is presented by Glouchtchenko [13]. Both the parafoil and the load are considered as a rigid body. The aerodynamic forces and gravity are separately modeled on both bodies. A suspension line model is proposed as a spring damper system. Four suspension lines are modeled into one single joint. The parafoil is connected to the joint with a half rigid and half spring damper connection. This brings as difficulty that the position of the joint is determined by solving the force balance of multiple spring damper systems. The aerodynamics are partly determined via a look-up map and with a linear model. The apparent mass is embedded in coupled form in the parafoil rigid body.

To conclude, the 3-4 DoF models are used when considering only steady-state flight dynamics, due to the constant aerodynamic coefficients. The turning response is an approximation with a delay. The 6 DoF models are used to consider the dynamic behavior of the system and has varying steady-state flight dynamics due to a more comprehensive aerodynamic model with varying aerodynamic coefficients. Due to the implementation of an inertia and the moments working on the system, the 6 DoF model can turn with all three Euler angles. A 7-9 DoF model is used to express some relative DoF between the load and the parafoil, these extra DoF can be constraint with spring-damper systems. A 12 DoF model give the load full relative movement freedom with respect of the parafoil, the relative DoF is constraint with multiple spring-damper

systems representing the tension lines. All presented models consider the gravity and the aerodynamics relevant for the flight dynamics of the PADS. The 6-12 DoF model considers a more comprehensive expression for the aerodynamics, than the 3-4 DoF models. In the 6-12 DoF models the aerodynamic coefficients can be modeled in a linear model, a look-up table or a mixture of both. The aerodynamic coefficients are obtained via analytical expressions, experimental result or CFD analyzes. The apparent mass is only included as relevant to the flight dynamics in the 6-12 DoF models. The apparent mass can be included in the 6-12 DoF models. Not all papers included the apparent mass, based on the application. The apparent mass is included in to manners. The first one considers the momentum and angular momentum of the apparent mass to be decoupled, while the second approach considers it coupled. The apparent mass is discussed further in Sec. 2.2.

2.2 Apparent mass effect

The apparent mass effect on a PADS is described by Lissaman and Brown [14] and by Barrows [15]. Here Lissaman and Brown [14] describes the relevance of the apparent mass effect on parafoil-load systems as: 'very significant for vehicles with wing load of the order less than 5 $[Kg/m^2]$ and exceedingly important if the lifting surface is significantly displaced from the major mass'. They derive in [14] representations, which approximates the effect with a diagonal mass matrix and diagonal inertia matrix. As result the momentum and angular momentum of the apparent mass are decoupled. The paper also shows how to derive the mass and inertia matrix. Barrows shows in [15] that for an arced parafoil system the decoupled from is in general not true. The paper presents a method to determine coupled representation of the force and moment equations. Also additions to calculated the coupled mass and inertia matrix are presented. In a PADS model the apparent mass effect is of importance, since the lifting surface is significantly displaced from the major mass. The decoupled form is still used as a simpler approximation of the apparent mass, It disregards of diagonal term between the mass and inertia matrix.

2.3 Aerodynamics

One of the most important parts of the model is the set of aerodynamic forces and moments, which depend on the aerodynamic coefficients. Obtaining the aerodynamic coefficients or an expression for the coefficients is not trivial. For airplane wings the lifting line theory is suitable to derive the aerodynamic coefficients [16], but this theory does not full capture the aerodynamic effect of a parafoil [17]. Bennett and Fox [18] describes how a set of coefficient is obtained experimentally. On the basis of this, Lingard [17] and Jann [16] try to extend the lifting line theory with the experimental results. They tried to obtain a general expression based on the parafoil geometry. It is shown that the theory matches the experimental results within a certain regions. Müller [19] describes a software tool in which the aerodynamic coefficients can be obtained numerically through CFD. The tool is verified with test flight data. In general all methods give set of coefficients suitable for an PADS model within a operation range. The CFD method can be scaled easily.

2.4 Experimental results and validation

Although the papers, given in Sec 2.1-2.3 present a model. Neither of those papers present a full set of simulation parameters as well as a full set of simulation results or experimental data. Most

papers present the model as part of a developed control strategy and only show results related to the control solution. Some papers present a complete set of model parameters like [20], but not an extensive set of result to validate the model with. Other papers present simulation or experiment results, but not enough of the used model parameter as in [7] and [18]. Glouchtchenko [13] gives a model validation based on simulations made by Van der Kolf [21], who gives a complete set of parameters including a extensive set of aerodynamic parameters. Multiple typos where found in the aerodynamic parameters. Van der Kolf presents data of both steady state flight behavior and dynamic flight behavior. The model Van der Kolf is simulating is a 8 DoF model, but his data can be used to validate general dynamics.

3 Analytical Model

In this section the analytical models are derived. First the reference frames are introduced. The orientation, velocity and angular velocity vectors are defined and the rotation matrices are given. The aerodynamic model, apparent mass and tension line model are described next. Then the 6 DoF model and the 12 DoF models are derived. Lastly, the general model is composted. The model is created using [4], [8], [2] and [9]. These models represents the PADS as one rigid body. With the use of [22] and [13] the 6 DoF model is extended to a 12 DoF model in which the parafoil and the payload are considered as two separate rigid bodies. The two bodies are connected with tension lines. The PADS system is shown as a schematic representation in Figure 2. The following assumptions are made

- The parafoil is treated as a rigid body of fixed shape once completely inflated.
- The apparent mass center corresponds to the parafoils center of mass.
- The earth is considered flat and to be non-rotating.
- The air density is considered a constant.

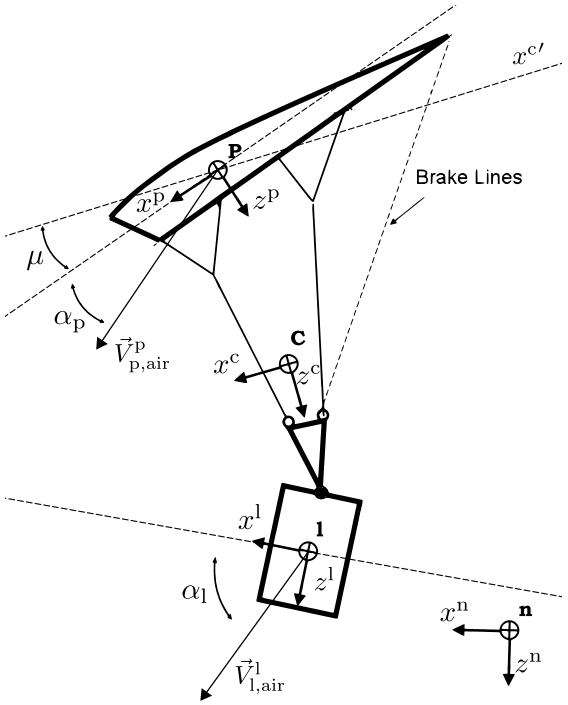

Figure 2: Schematic representation of PADS

3.1 Reference frames and rotations

Four reference frames are defined for modeling purposes. The reference frames are shown in Figure 2 and the reference frames will be denoted with a super script. The first frame is the North-East-Down or world frame denoted by {n}, which is an inertial frame fixed in a planetary

point. The frame axis are denoted as x^{n}, y^{n} and z^{n}. The x^{n} axis is positive towards the north, the y^{n} axis is positive towards the east and the z^{n} axis is positive pointing towards the center of the planet.

The model is derived in a body fixed frame. Three body fixed reference frames will be used. Firstly, a body fixed frame in the center of mass of the rigid body will be used for the 6 DoF model. This frame is denoted with {c}, with the axis x^{c} positive along the longitudinal axis of the PADS in the plane of symmetry, the z^{c} axis is perpendicular to the x^{c} axis positive pointing down and the y^{c} axis is perpendicular to the x^{c}-z^{c} plane, positive defined by the right-hand rule.

Secondly, a body fixed frame is used in the center of mass of the parafoil, denoted with {p}. The axis x^{p} is positive along the longitudinal axis of the parafoil in the plane of symmetry, the z^{p} axis is perpendicular to the x^{p} axis positive pointing down and the y^{p} axis is perpendicular to the x^{p}-z^{p} plane positive defined by the right-hand rule.

Lastly, a body fixed frame is placed in the center of mass of the load. The frame is denoted with {l} and the axis x^{l} is positive along the longitudinal axis of the load in the plane of symmetry, the z^{l} axis is perpendicular to the x^{l} axis positive pointing down and the y^{l} axis is perpendicular to the x^{l}-z^{l} plane positive defined by the right-hand rule.

In each body fixed frame the orientation w.r.t. the {n} frame can be represented in Euler angles. The angle ϕ represents a rotation around the x-axis, θ a rotation around the y-axis and ψ a rotation around the z-axis. This is summarized as $\vec{\eta} = \begin{bmatrix} \phi & \theta & \psi \end{bmatrix}^\top$. In a body fixed frame these angles could also be referred to as roll, pitch and yaw. μ is a specific defined angle. It describes the relative rotation between the parafoil frame and the rigid body frame around the y-axis. The meaning of μ is also shown in Figure 2. The velocity in each frames is denoted with $(\vec{V})$ and is decomposed in $\begin{bmatrix} u & v & w \end{bmatrix}^\top$. The angular velocity $\vec{\omega}$ is decomposed as $\begin{bmatrix} p & q & r \end{bmatrix}^\top$. The time derivative of the Euler angles of an arbitrary body fixed frame {b} can be determined as

$$\frac{d\vec{\eta}^{\mathrm{b}}}{dt}(\vec{\omega}^{\mathrm{b}}, \vec{\eta}^{\mathrm{b}}) = \underbrace{\begin{bmatrix} 1 & \sin(\phi^{\mathrm{b}})\tan(\theta^{\mathrm{b}}) & \cos(\phi^{\mathrm{b}})\tan(\theta^{\mathrm{b}}) \\ 0 & \cos(\phi^{\mathrm{b}}) & -\sin(\phi^{\mathrm{b}}) \\ 0 & -\sin(\phi^{\mathrm{b}})\frac{1}{\cos(\theta^{\mathrm{b}})} & \cos(\phi^{\mathrm{b}})\frac{1}{\cos(\theta^{\mathrm{b}})} \end{bmatrix}}_{T} \vec{\omega}^{\mathrm{b}}. \tag{1}$$

Any vector in a frame can be rotated to another frame with the Euler angles by multiplying with one or multiple of the corresponding matrices as

$$\begin{gathered} R(\psi^{\mathrm{b}}) = \begin{bmatrix} \cos(\psi^{\mathrm{b}}) & \sin(\psi^{\mathrm{b}}) & 0 \\ -\sin(\psi^{\mathrm{b}}) & \cos(\psi^{\mathrm{b}}) & 0 \\ 0 & 0 & 1 \end{bmatrix}, \qquad R(\theta^{\mathrm{b}}) = \begin{bmatrix} \cos(\theta^{\mathrm{b}}) & 0 & -\sin(\theta^{\mathrm{b}}) \\ 0 & 1 & 0 \\ \sin(\theta^{\mathrm{b}}) & 0 & \cos(\theta^{\mathrm{b}}) \end{bmatrix}, \\ R(\phi^{\mathrm{b}}) = \begin{bmatrix} 1 & 0 & 0 \\ 0 & \cos(\phi^{\mathrm{b}}) & \sin(\phi^{\mathrm{b}}) \\ 0 & -\sin(\phi^{\mathrm{b}}) & \cos(\phi^{\mathrm{b}}) \end{bmatrix}, \end{gathered} \tag{2}$$

such that a rotation with al three Euler angles would result in

$$R(\vec{\eta}^{\,\mathrm{b}}) = R(\psi^{\mathrm{b}})R(\theta^{\mathrm{b}})R(\phi^{\mathrm{b}}). \tag{3}$$

The rotation order matters and is defined as above. By using Euler angles there is a chance that gimbal lock will occur in the model. If for instance, if the angle θ becomes $\frac{1}{2}\pi$ the rotation

matrices lose a degree of freedom and also its rank. A rotation with ϕ or ψ will result in the same rotation around the z-axis, but a rotation around the x-axis is not possible. The model for the PADS should not operate at $\theta = \frac{1}{2}\pi$, in normal operation conditions, but it is possible. This phenomena is avoided by expressing the orientation in quaternions. Quaternions are a generalization of the complex numbers and are formally written as $q_0 + q_1 i + q_2 j + q_3 k$. q_i is a real number. i, j, k are the direction vectors. The properties of i, j, k are given in [23]. By using quaternion w.r.t Euler angles an intuitive understanding of the angle is lost. Therefore, the model is presented in Euler angles, but implemented in SIMULINK in quaternions. The orientation in quaternions is described as $\vec{q} = \begin{bmatrix} q_0 & q_1 & q_2 & q_3 \end{bmatrix}^\top$. A vector can be rotated from the world frame to an arbitrary body fixed frame {b} with the rotation matrix following [23] defined as

$$R(\vec{q}^{\,\mathrm{b}}) = \begin{bmatrix} (q_0^{\mathrm{b}})^2 + (q_1^{\mathrm{b}})^2 - (q_2^{\mathrm{b}})^2 - (q_3^{\mathrm{b}})^2 & 2\left(q_1^{\mathrm{b}} q_2^{\mathrm{b}} - q_0^{\mathrm{b}} q_3^{\mathrm{b}}\right) & 2\left(q_0^{\mathrm{b}} q_2^{\mathrm{b}} + q_1^{\mathrm{b}} q_3^{\mathrm{b}}\right) \\ 2\left(q_0^{\mathrm{b}} q_3^{\mathrm{b}} + q_1^{\mathrm{b}} q_2^{\mathrm{b}}\right) & (q_0^{\mathrm{b}})^2 - (q_1^{\mathrm{b}})^2 + (q_2^{\mathrm{b}})^2 - (q_3^{\mathrm{b}})^2 & 2\left(q_2^{\mathrm{b}} q_3^{\mathrm{b}} - q_0^{\mathrm{b}} q_1^{\mathrm{b}}\right) \\ 2\left(q_1^{\mathrm{b}} q_3^{\mathrm{b}} - q_0^{\mathrm{b}} q_2^{\mathrm{b}}\right) & 2\left(q_0^{\mathrm{b}} q_1^{\mathrm{b}} + q_2^{\mathrm{b}} q_3^{\mathrm{b}}\right) & (q_0^{\mathrm{b}})^2 - (q_1^{\mathrm{b}})^2 - (q_2^{\mathrm{b}})^2 + (q_3^{\mathrm{b}})^2 \end{bmatrix}. \tag{4}$$

The time derivative of the quaternion representation $\vec{q}^{\,\mathrm{b}}$ for an arbitrary body fixed frame {b} is given as

$$\frac{d\vec{q}^{\,\mathrm{b}}}{dt}(\vec{\omega}^{\mathrm{b}}, \vec{q}^{\,\mathrm{b}}) = \frac{1}{2} \begin{bmatrix} -q_1^{\mathrm{b}} & -q_2^{\mathrm{b}} & -q_3^{\mathrm{b}} \\ q_0^{\mathrm{b}} & -q_3^{\mathrm{b}} & q_2^{\mathrm{b}} \\ q_3^{\mathrm{b}} & q_0^{\mathrm{b}} & -q_1^{\mathrm{b}} \\ -q_2^{\mathrm{b}} & q_1^{\mathrm{b}} & q_0^{\mathrm{b}} \end{bmatrix} \vec{\omega}^{\mathrm{b}}. \tag{5}$$

3.2 Aerodynamics

The aerodynamics of the PADS system can be separated in the aerodynamics of the parafoil and the load, working in the parafoil frame and load frame respectively. The aerodynamics of the parafoil are described with the parafoil aerodynamic force ($\vec{F}^{\mathrm{p}}_{\mathsf{p_a}}$) and moment ($\vec{M}^{\mathrm{p}}_{\mathsf{p_a}}$) as

$$\begin{aligned} \vec{F}^{\mathrm{p}}_{\mathsf{p_a}}(\vec{V}^{\mathrm{p}}_{\mathrm{p,air}}, \vec{\omega}^{\mathrm{p}}_{\mathrm{p}}, \delta_{\mathrm{r}}, \delta_{\mathrm{l}}) &= \frac{\rho ||\vec{V}^{\mathrm{p}}_{\mathrm{p,air}}||_2^2 S_{\mathrm{p}}}{2} R(\alpha_{\mathrm{p}}, \beta_{\mathrm{p}}) C_{\mathrm{Fp}}(\alpha_{\mathrm{p}}, \beta_{\mathrm{p}}, \vec{V}^{\mathrm{p}}_{\mathrm{p,air}}, \vec{\omega}^{\mathrm{p}}_{\mathrm{p}}, \delta_{\mathrm{r}}, \delta_{\mathrm{l}}), \\ \vec{M}^{\mathrm{p}}_{\mathsf{p_a}}(\vec{V}^{\mathrm{p}}_{\mathrm{p,air}}, \vec{\omega}^{\mathrm{p}}_{\mathrm{p}}, \delta_{\mathrm{r}}, \delta_{\mathrm{l}}) &= \frac{\rho ||\vec{V}^{\mathrm{p}}_{\mathrm{p,air}}||_2^2 S_{\mathrm{p}}}{2} C_{\mathrm{Mp}}(\alpha_{\mathrm{p}}, \beta_{\mathrm{p}}, \vec{V}^{\mathrm{p}}_{\mathrm{p,air}}, \vec{\omega}^{\mathrm{p}}_{\mathrm{p}}, \delta_{\mathrm{r}}, \delta_{\mathrm{l}}), \\ \alpha_{\mathrm{p}} &= \tan^{-1}\left(\frac{w^{\mathrm{p}}_{\mathrm{p,air}}}{u^{\mathrm{p}}_{\mathrm{p,air}}}\right), \\ \beta_{\mathrm{p}} &= \tan^{-1}\left(\frac{v^{\mathrm{p}}_{\mathrm{p,air}}}{\sqrt{{u^{\mathrm{p}}_{\mathrm{p,air}}}^2 + {w^{\mathrm{p}}_{\mathrm{p,air}}}^2}}\right), \end{aligned} \tag{6}$$

here ρ is the air density, S_{p} is the aerodynamic reference area of the parafoil, $\vec{V}^{\mathrm{p}}_{\mathrm{p,air}}$ is the air velocity of the parafoil. α_{p} is the angle of attack of the parafoils air velocity and β_{p} is the sideslip angle of the parafoil air velocity. $\vec{\omega}^{\mathrm{p}}_{\mathrm{p}}$ is the angular velocity of the parafoil. C_{Fp} and C_{Mp} are the vectors with aerodynamic coefficients for the parafoil. δ_{r} and δ_{l} are the relative right and left parafoil deflection respectively. The aerodynamics of the load are described in the same manner

with the aerodynamic force ($\vec{F}^{\mathrm{l}}_{\mathrm{l_a}}$) and the aerodynamic moment ($\vec{M}^{\mathrm{l}}_{\mathrm{l_a}}$) as

$$\begin{aligned}
\vec{F}^{\mathrm{l}}_{\mathrm{l_a}}(\vec{V}^{\mathrm{l}}_{\mathrm{l,air}}, \vec{\omega}^{\mathrm{l}}_{\mathrm{l}}) &= \frac{\rho||\vec{V}^{\mathrm{l}}_{\mathrm{l,air}}||^2_2 S_{\mathrm{l}}}{2} R(\alpha_{\mathrm{l}}, \beta_{\mathrm{l}}) C_{\mathrm{Fl}}(\alpha_{\mathrm{l}}, \beta_{\mathrm{l}}, \vec{V}^{\mathrm{l}}_{\mathrm{l,air}}, \vec{\omega}^{\mathrm{l}}_{\mathrm{l}}), \\
\vec{M}^{\mathrm{l}}_{\mathrm{l_a}}(\vec{V}^{\mathrm{l}}_{\mathrm{l,air}}, \vec{\omega}^{\mathrm{l}}_{\mathrm{l}}) &= \frac{\rho||\vec{V}^{\mathrm{l}}_{\mathrm{l,air}}||^2_2 S_{\mathrm{l}}}{2} C_{\mathrm{Ml}}(\alpha_{\mathrm{l}}, \beta_{\mathrm{l}}, \vec{V}^{\mathrm{l}}_{\mathrm{l,air}}, \vec{\omega}^{\mathrm{l}}_{\mathrm{l}}), \\
\alpha_{\mathrm{l}} &= \tan^{-1}\left(\frac{w^{\mathrm{l}}_{\mathrm{l,air}}}{u^{\mathrm{l}}_{\mathrm{l,air}}}\right), \\
\beta_{\mathrm{l}} &= \tan^{-1}\left(\frac{v^{\mathrm{l}}_{\mathrm{l,air}}}{\sqrt{u^{\mathrm{l}2}_{\mathrm{l,air}} + w^{\mathrm{l}2}_{\mathrm{l,air}}}}\right),
\end{aligned} \tag{7}$$

here $\vec{V}^{\mathrm{l}}_{\mathrm{l,air}}$ is the air velocity of the load, α_{l} and β_{l} are the angle of attack and the slideslip angle of the load. $\vec{\omega}^{\mathrm{l}}_{\mathrm{l}}$ is the angular velocity of the load. C_{Fl} and C_{Ml} are the vectors with the aerodynamic coefficients of the load. It should be noted that depending on the geometry of the load the given expression may be over complicated. Depending on the geometry, it could be that the lift and side component are not significant and only the drag component is considered.

The aerodynamic coefficients can be obtained through the lifting line theory [24], [16], computed from measurement data [18] or calculated via Computational Fluid Dynamics (CFD) [19], [2]. The coefficients are highly nonlinear and dependent on a lot of different variables. Different papers use different manners to implement this. One of the solutions is a linearization around an operation point as is used in [9]. The other end of the spectrum is the use of a look-up table in which the coefficients for specific variables will be obtained through interpolation on known data as is used in [2]. A lot of papers use a mixture between both methods. [10] developed a linearization in a moving operation point. The dependencies chosen for the aerodynamic coefficients are α, β, the dimensionless angular velocity ($\bar{\omega}$), the symmetrical deflection (δ_{s}), and the asymmetric deflection (δ_{a}). For an arbitrary reference frame {b}, the dimensionless angular velocity is given as

$$\begin{bmatrix} \bar{p}^{\mathrm{b}} \\ \bar{q}^{\mathrm{b}} \\ \bar{r}^{\mathrm{b}} \end{bmatrix} = \frac{1}{2||\vec{V}^{\mathrm{b}}_{\mathrm{b,air}}||} \begin{bmatrix} b_{\mathrm{b}} p^{\mathrm{b}} \\ c_{\mathrm{b}} q^{\mathrm{b}} \\ b_{\mathrm{b}} r^{\mathrm{b}} \end{bmatrix}. \tag{8}$$

The symmetric and asymmetric deflection (δ_{s}) and (δ_{a}) are determined as

$$\delta_{\mathrm{s}} = \min(\delta_{\mathrm{r}}, \delta_{\mathrm{l}}) \quad \delta_{\mathrm{a}} = \delta_{\mathrm{r}} - \delta_{\mathrm{l}}. \tag{9}$$

The aerodynamic coefficients for the parafoil used in this research are given as follows,

$$\begin{aligned}
C_{\mathrm{Fp}} &= \begin{bmatrix} -C_{\mathrm{D,p}} \\ C_{\mathrm{Y,p}} \\ -C_{\mathrm{L,p}} \end{bmatrix} = \begin{bmatrix} -C_{\mathrm{D,p}}(\alpha_{\mathrm{p}}, \delta_{\mathrm{s}}) \\ C_{\mathrm{Y}\beta,\mathrm{p}}\beta_{\mathrm{p}} + C_{\mathrm{Yp,p}}\bar{p}^{\mathrm{p}} + C_{\mathrm{Yr,p}}\bar{r}_{\mathrm{p}} + C_{\mathrm{Y}\delta_{\mathrm{a}},\mathrm{p}}\delta_{\mathrm{a}} \\ -C_{\mathrm{L,p}}\left(\alpha_{\mathrm{p}}, \delta_{\mathrm{s}}\right) \end{bmatrix}, \\
C_{\mathrm{Mp}} &= \begin{bmatrix} C_{\mathrm{l,p}} \\ C_{\mathrm{m,p}} \\ C_{\mathrm{n,p}} \end{bmatrix} = \begin{bmatrix} C_{\mathrm{l}\beta,\mathrm{p}}\beta_{\mathrm{p}} + C_{\mathrm{lp,p}}\bar{p}^{\mathrm{p}} + C_{\mathrm{lr,p}}\bar{r}^{\mathrm{p}} + C_{\mathrm{l}\delta_{\mathrm{a}},\mathrm{p}}\delta_{\mathrm{a}} \\ C_{\mathrm{m,p}}\left(\alpha_{\mathrm{p}}, \delta_{\mathrm{s}}\right) + C_{\mathrm{mq,p}}\bar{q}^{\mathrm{p}} \\ C_{\mathrm{n}\beta,\mathrm{p}}\beta_{\mathrm{p}} + C_{\mathrm{np,p}}\bar{p}^{\mathrm{p}} + C_{\mathrm{nr,p}}\bar{r}^{\mathrm{p}} + C_{\mathrm{n}\delta_{\mathrm{a}},\mathrm{p}}(\delta_{\mathrm{s}}, \delta_{\mathrm{a}}) \end{bmatrix}
\end{aligned} \tag{10}$$

which is a mixture between a linear model and a lookup table. The aerodynamic coefficients for the load are given via a linear model as

$$
\begin{aligned}
C_{\mathrm{Fl}} &= \begin{bmatrix} -C_{\mathrm{D,l}} \\ C_{\mathrm{Y,l}} \\ -C_{\mathrm{L,l}} \end{bmatrix} = \begin{bmatrix} -C_{\mathrm{D0,l}} - C_{\mathrm{D}\alpha,\mathrm{l}}\alpha_{\mathrm{l}}^2 \\ C_{\mathrm{Y}\beta,\mathrm{l}}\beta_{\mathrm{l}} \\ -C_{\mathrm{L0,l}} - C_{\mathrm{L}\alpha,\mathrm{l}}\alpha_{\mathrm{l}} \end{bmatrix}, \\
C_{\mathrm{Ml}} &= \begin{bmatrix} C_{\mathrm{l,l}} \\ C_{\mathrm{m,l}} \\ C_{\mathrm{n,l}} \end{bmatrix} = \begin{bmatrix} C_{\mathrm{l}\beta,\mathrm{l}}\beta_{\mathrm{l}} + C_{\mathrm{mp,l}}\bar{p}^{\mathrm{l}} + C_{\mathrm{mr,l}}\bar{r}^{\mathrm{l}} \\ C_{\mathrm{m0,l}} + C_{\mathrm{m}\alpha,\mathrm{l}}\alpha_{\mathrm{l}} + C_{\mathrm{mq,l}}\bar{q}^{\mathrm{l}} \\ C_{\mathrm{n}\beta,\mathrm{l}}\beta_{\mathrm{l}} + C_{\mathrm{np,l}}\bar{p}^{\mathrm{l}} + C_{\mathrm{nr,l}}\bar{r}^{\mathrm{l}} \end{bmatrix}.
\end{aligned}
\tag{11}
$$

3.3 Apparent mass

The apparent mass describes the effect of an moving body through a fluid and setting the fluid in motion. The moving fluid results in pressure forces on the body. Therefore, the body takes additional energy to move [14]. The effect is not widely used in all applications for a body moving through fluid or air. The apparent mass effect is minimal if the mass of the body is much larger than the mass of the air set into motion. For lighter than air vehicles and parachutes this effect can be significant. For systems in which the lifting surface is significantly displaced from the major mass, the apparent mass effect is exceedingly important [14]. Lissaman and Brown describe in [14] how the energy of the moving fluid can be captured as

$$
2T = Au^2 + Bv^2 + Cw^2 + I_A p^2 + I_B q^2 + I_C r^2. \tag{12}
$$

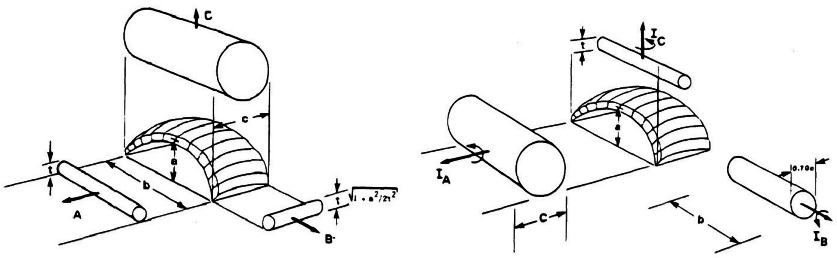

Figure 3: Volumetric Representation of the apparent mass (Lissaman and Brown) [14]

From here on it is assumes that the mass of the moving fluid is capture in an ellipsoidal body. For each direction a different ellipsoidal body is modeled, as shown in Figure 3. One apparent mass center is found such that the apparent mass matrix ($m^{\mathrm{p}}_{\mathsf{p}_{\mathrm{m}}}$) and the apparent inertia matrix ($I^{\mathrm{p}}_{\mathsf{p}_{\mathrm{m}}}$) are defined as

$$
m^{\mathrm{p}}_{\mathsf{p}_{\mathrm{m}}} = \begin{bmatrix} A & 0 & 0 \\ 0 & B & 0 \\ 0 & 0 & C \end{bmatrix} \quad I^{\mathrm{p}}_{\mathsf{p}_{\mathrm{m}}} = \begin{bmatrix} I_{\mathrm{A}} & 0 & 0 \\ 0 & I_{\mathrm{B}} & 0 \\ 0 & 0 & I_{\mathrm{C}} \end{bmatrix}. \tag{13}
$$

In [14] expressions are given to determined the apparent mass and inertia matrices. The resulting force ($\vec{F}^{\mathrm{p}}_{\mathsf{p}_{\mathrm{m}}}$) and moment ($\vec{M}^{\mathrm{p}}_{\mathsf{p}_{\mathrm{m}}}$) of the moving mass in the body are expressed as

$$
\vec{F}^{\mathrm{p}}_{\mathsf{p}_{\mathrm{m}}}\left(\frac{d\vec{V}^{\mathrm{p}}_{\mathrm{p,air}}}{dt}, \vec{V}^{\mathrm{p}}_{\mathrm{p,air}}, \vec{\omega}^{\mathrm{p}}_{\mathrm{p}}\right) = -m^{\mathrm{p}}_{\mathsf{p}_{\mathrm{m}}}\frac{d\vec{V}^{\mathrm{p}}_{\mathrm{p,air}}}{dt} - \vec{\omega}^{\mathrm{p}}_{\mathrm{p}} \times m^{\mathrm{p}}_{\mathsf{p}_{\mathrm{m}}}\vec{V}^{\mathrm{p}}_{\mathrm{p,air}} \tag{14}
$$

and

$$\vec{M}^{\mathrm{p}}_{\mathsf{p}_\mathrm{m}}\left(\frac{d\vec{\omega}^{\mathrm{p}}_{\mathrm{p}}}{dt},\vec{V}^{\mathrm{p}}_{\mathrm{p,air}},\vec{\omega}^{\mathrm{p}}_{\mathrm{p}}\right)=-I^{\mathrm{p}}_{\mathsf{p}_\mathrm{m}}\frac{d\vec{\omega}^{\mathrm{p}}_{\mathrm{p}}}{dt}-\vec{V}^{\mathrm{p}}_{\mathrm{p,air}}\times m^{\mathrm{p}}_{\mathsf{p}_\mathrm{m}}\vec{V}^{\mathrm{p}}_{\mathrm{p,air}}-\vec{\omega}^{\mathrm{p}}_{\mathrm{p}}\times I^{\mathrm{p}}_{\mathsf{p}_\mathrm{m}}\vec{\omega}^{\mathrm{p}}_{\mathrm{p}}. \tag{15}$$

where $\vec{V}^{\mathrm{p}}_{\mathrm{p,air}}$ is the parafoil velocity. The term $\vec{V}^{\mathrm{p}}_{\mathrm{p,air}}\times m^{\mathrm{p}}_{\mathsf{p}_\mathrm{m}}\vec{V}^{\mathrm{p}}_{\mathrm{p,air}}$ can be neglected as it may also be considered in the aerodynamics [4], [11]. Following Yakimenko [4] $\frac{d\vec{V}^{\mathrm{p}}_{\mathrm{p,air}}}{dt}=\frac{d\vec{V}^{\mathrm{p}}_{\mathrm{p}}}{dt}$. The time dependency of the wind vector and the orientation are disregarded. Barrows argues in [15] that in general finding one single center of apparent mass is not trivial. Therefore, it is impossible to decouple the equations of motion in one single point. A total apparent momentum ($\vec{P}^{\mathrm{p}}_{\mathsf{p}_\mathrm{m}}$) and angular momentum ($\vec{H}^{\mathrm{p}}_{\mathsf{p}_\mathrm{m}}$) is found as

$$\begin{bmatrix}\vec{P}^{\mathrm{p}}_{\mathsf{p}_\mathrm{m}}\\ \vec{H}^{\mathrm{p}}_{\mathsf{p}_\mathrm{m}}\end{bmatrix}=\begin{bmatrix}m^{\mathrm{p}}_{\mathsf{p}_\mathrm{m}} & D^{\mathrm{p}}_{\mathsf{p}_\mathrm{m}}\\ D^{\mathrm{p}\top}_{\mathsf{p}_\mathrm{m}} & I^{\mathrm{p}}_{\mathsf{p}_\mathrm{m}}\end{bmatrix}\begin{bmatrix}\vec{V}^{\mathrm{p}}_{\mathrm{p,air}}\\ \vec{\omega}^{\mathrm{p}}_{\mathrm{p}}\end{bmatrix}, \tag{16}$$

with $D^{\mathrm{p}}_{\mathsf{p}_\mathrm{m}}$ as a matrix with the coupling terms. The resulting force and moment can be written as

$$\vec{F}^{\mathrm{p}}_{\mathsf{p}_\mathrm{m}}\left(\frac{d\vec{V}^{\mathrm{p}}_{\mathrm{p,air}}}{dt},\frac{d\vec{\omega}^{\mathrm{p}}_{\mathrm{p}}}{dt},\vec{V}^{\mathrm{p}}_{\mathrm{p,air}},\vec{\omega}^{\mathrm{p}}_{\mathrm{p}}\right)=-m^{\mathrm{p}}_{\mathsf{p}_\mathrm{m}}\frac{d\vec{V}^{\mathrm{p}}_{\mathrm{p,air}}}{dt}-D^{\mathrm{p}}_{\mathsf{p}_\mathrm{m}}\frac{d\vec{\omega}^{\mathrm{p}}_{\mathrm{p}}}{dt}-\vec{\omega}^{\mathrm{p}}_{\mathrm{p}}\times m^{\mathrm{p}}_{\mathsf{p}_\mathrm{m}}(\vec{V}^{\mathrm{p}}_{\mathrm{p,air}}-D^{\mathrm{p}}_{\mathsf{p}_\mathrm{m}}\vec{\omega}^{\mathrm{p}}_{\mathrm{p}}) \tag{17}$$

and

$$\begin{aligned}\vec{M}^{\mathrm{p}}_{\mathsf{p}_\mathrm{m}}\left(\frac{d\vec{V}^{\mathrm{p}}_{\mathrm{p,air}}}{dt},\frac{d\vec{\omega}^{\mathrm{p}}_{\mathrm{p}}}{dt},\vec{V}^{\mathrm{p}}_{\mathrm{p,air}},\vec{\omega}^{\mathrm{p}}_{\mathrm{p}}\right)=&-D^{\mathrm{p}\top}_{\mathsf{p}_\mathrm{m}}\frac{d\vec{V}^{\mathrm{p}}_{\mathrm{p,air}}}{dt}-I^{\mathrm{p}}_{\mathsf{p}_\mathrm{m}}\frac{d\vec{\omega}^{\mathrm{p}}_{\mathrm{p}}}{dt}-\vec{V}^{\mathrm{p}}_{\mathrm{p,air}}\times m^{\mathrm{p}}_{\mathsf{p}_\mathrm{m}}(\vec{V}^{\mathrm{p}}_{\mathrm{p,air}}-D^{\mathrm{p}}_{\mathsf{p}_\mathrm{m}}\vec{\omega}^{\mathrm{p}}_{\mathrm{p}})\\ &-\vec{\omega}^{\mathrm{p}}_{\mathrm{p}}\times m^{\mathrm{p}}_{\mathsf{p}_\mathrm{m}}D^{\mathrm{p}\top}_{\mathsf{p}_\mathrm{m}}\vec{V}^{\mathrm{p}}_{\mathrm{p,air}}-\vec{\omega}^{\mathrm{p}}_{\mathrm{p}}\times I^{\mathrm{p}}_{\mathsf{p}_\mathrm{m}}\vec{\omega}^{\mathrm{p}}_{\mathrm{p}}\end{aligned} \tag{18}$$

Despite of this [4, 7, 8, 20] all assume that a single centroid for the apparent mass can be found. For simplicity and to study the added effect of the apparent mass, this approach will be used in this research.

3.4 Tension line model

In the 12 DoF model, a tension line model connects the parafoil to the load. The tension lines are modeled as a spring-damper system, with an equilibrium vector. The tension line can be stretched and compressed in each direction separately with a different spring and damping constant. The equilibrium vector is equal to the relative position vector of the the load w.r.t. the parafoil. On top a torsion spring-damper system is used to constrain the relative rotation between the bodies. For each angle a different stiffness and damping is set. The parafoil tension force ($\vec{F}^{\mathrm{p}}_{\mathsf{p}_\mathrm{t}}$) and moment ($\vec{M}^{\mathrm{p}}_{\mathsf{p}_\mathrm{t}}$) are represented as

$$\begin{aligned}\vec{F}^{\mathrm{p}}_{\mathsf{p}_\mathrm{t}}\left(\vec{r}^{\,\mathrm{p}}_{\mathrm{t}},\frac{d\vec{r}^{\,\mathrm{p}}_{\mathrm{t}}}{dt}\right)&=-K_{\mathrm{t},\vec{r}}(\vec{r}^{\,\mathrm{p}}_{\mathrm{t}}-\vec{r}^{\,\mathrm{p}}_{\mathrm{eq}})-D_{\mathrm{t},\vec{r}}\left(\frac{d\vec{r}^{\,\mathrm{p}}_{\mathrm{t}}}{dt}\right),\\ \vec{M}^{\mathrm{p}}_{\mathsf{p}_\mathrm{t}}\left(\vec{\eta}^{\,\mathrm{t}},\frac{d\vec{\eta}^{\,\mathrm{t}}}{dt}\right)&=-K_{\mathrm{t},\vec{\eta}}(\vec{\eta}^{\,\mathrm{t}}-\vec{\eta}^{\,\mathrm{eq}})-D_{\mathrm{t},\vec{\eta}}\left(\frac{d\vec{\eta}^{\,\mathrm{t}}}{dt}\right),\end{aligned} \tag{19}$$

in which $K_{\mathrm{t},\vec{r}}$ is diag($[k_{\mathrm{t,x}}\ \ k_{\mathrm{t,y}}\ \ k_{\mathrm{t,z}}]$) with the stiffness coefficients and $D_{\mathrm{t},\vec{r}}$ is diag($[d_{\mathrm{t,x}}\ \ d_{\mathrm{t,y}}\ \ d_{\mathrm{t,z}}]$) with damping coefficients. $\vec{r}^{\,\mathrm{p}}_{\mathrm{t}}$ is the relative position vector w.r.t. to the parafoil. $K_{\mathrm{t},\vec{\eta}}$ is

$\text{diag}([k_{\text{t},\phi} \;\; k_{\text{t},\theta} \;\; k_{\text{t},\psi}])$ with stiffness coefficients and $D_{\text{t},\vec{\eta}}$ is $\text{diag}([d_{\text{t},\phi} \;\; d_{\text{t},\theta} \;\; d_{\text{t},\psi}])$ with damping coefficients. $\vec{\eta}^{\,\text{t}}$ is the load orientation w.r.t. the parafoil. The tension force ($\vec{F}^{\text{l}}_{\text{l}_\text{t}}$) and moment ($\vec{M}^{\text{l}}_{\text{l}_\text{t}}$) acting on the load and are expressed as

$$\begin{aligned}\vec{F}^{\text{l}}_{\text{l}_\text{t}}\left(\vec{r}^{\,\text{p}}_{\text{t}}, \vec{\eta}^{\,\text{t}}, \frac{d\vec{r}^{\,\text{p}}_{\text{t}}}{dt}\right) &= -R(\vec{\eta}^{\,\text{t}})^\top \vec{F}^{\text{p}}_{\text{p}_\text{t}}\left(\vec{r}^{\,\text{p}}_{\text{t}}, \frac{d\vec{r}^{\,\text{p}}_{\text{t}}}{dt}\right),\\ \vec{M}^{\text{l}}_{\text{l}_\text{t}}\left(\vec{\eta}^{\,\text{t}}, \frac{d\vec{\eta}^{\,\text{t}}}{dt}\right) &= -R(\vec{\eta}^{\,\text{t}})^\top \vec{M}^{\text{p}}_{\text{p}_\text{t}}\left(\vec{\eta}^{\,\text{t}}, \frac{d\vec{\eta}^{\,\text{t}}}{dt}\right).\end{aligned} \tag{20}$$

3.5 Six DoF model of PADS flight dynamics

As mentioned earlier, the 6 DoF model describes the PADS system as one rigid body with one mass and one inertia in the CoM of the system. Therefore, the masses the parafoil (m_p) and the load mass (m_l) is added as one mass (m_c). The parafoils inertia (I^p_p) and the load inertia (I^l_l) is added in one inertia in the CoM of the system (I^c_c). The total inertia is defined in the $\{\text{c}\}$ frame. The total mass in the CoM is found as

$$m_\text{c} = m_\text{p} + m_\text{l} \tag{21}$$

The inertia of the parafoil, which is defined in the parafoil frame, should be rotated with μ to express it in the $\{\text{c}\}$ frame. Then the total inertia in the CoM is determined as

$$\begin{aligned}I^\text{c}_\text{p} &= R(\mu)^\top (I^\text{p}_\text{p}) R(\mu) + m_\text{p}(\vec{r}^{\,\text{c}\top}_{\text{c,p}} \vec{r}^{\,\text{c}}_{\text{c,p}} I^{3\text{x}3} - \vec{r}^{\,\text{c}}_{\text{c,p}} \vec{r}^{\,\text{c}\top}_{\text{c,p}}),\\ I^\text{c}_\text{l} &= I^\text{l}_\text{l} + m_\text{l}(\vec{r}^{\,\text{c}\top}_{\text{c,l}} \vec{r}^{\,\text{c}}_{\text{c,l}} I^{3\text{x}3} - \vec{r}^{\,\text{c}}_{\text{c,l}} \vec{r}^{\,\text{c}\top}_{\text{c,l}}),\\ I^\text{c}_\text{c} &= I^\text{c}_\text{p} + I^\text{c}_\text{l},\end{aligned} \tag{22}$$

in which $\vec{r}^{\,\text{c}}_{\text{c,p}}$ is the position vector from the CoM to the parafoil mass and $\vec{r}^{\,\text{c}}_{\text{c,l}}$ is the position vector from the CoM to the load mass. $I^{3\text{x}3}$ is a 3 by 3 identity matrix. The position vector to the CoM ($\vec{r}^{\,\text{c}}_\text{c}$) is determined as

$$\vec{r}^{\,\text{c}}_\text{c} = m_\text{c}^{-1}\left(m_\text{p}\vec{r}^{\,\text{c}}_{\text{c,p}} + m_\text{l}\vec{r}^{\,\text{c}}_{\text{c,l}}\right) \tag{23}$$

when all the position vectors are correctly defined the CoM should be in the zero coordinate of the $\{\text{c}\}$ frame. The position vector from the CoM to the center of gravity is also zero. The equations of motion for the PADS modeled as one 6 DoF rigid body are dependent on the sum of forces and moments. The 6 DOF model has contributions from the parafoil aerodynamics (p_a), load aerodynamics (l_a), the gravity (g) and the apparent mass (p_m). An index set D is constructed as $\{\mathsf{p}_\text{a}, \mathsf{l}_\text{a}, \mathsf{g}, \mathsf{p}_\text{m}\}$ to sum all the contributions. The Equation of Motion (EoM) for the acceleration of the body is given as

$$m_\text{c}\frac{d\vec{V}^\text{c}_\text{c}}{dt} + \vec{\omega}^\text{c}_\text{c} \times m_\text{c}\vec{V}^\text{c}_\text{c} = \sum_{i\in D} \vec{F}^\text{c}_\text{i}\left(\frac{d\vec{V}^\text{c}_\text{c}}{dt}, \frac{d\vec{\omega}^\text{c}_\text{c}}{dt}, \vec{V}^\text{c}_\text{c}, \vec{\omega}^\text{c}, \vec{\eta}^{\,\text{c}}, \delta_\text{r}, \delta_\text{l}\right), \tag{24}$$

in which $\vec{V}^\text{c}_\text{c}$ is the body velocity in the CoM, $\vec{\omega}^\text{c}_\text{c}$ is the body angular velocity in the CoM and $\vec{\eta}^{\,\text{c}}$ is the orientation w.r.t. the world frame of the body. $\vec{F}^\text{c}_\text{i}$ represents a contributing force in the index set of D. The EoM for the angular acceleration is given as

$$I^\text{c}_\text{c}\frac{d\vec{\omega}^\text{c}_\text{c}}{dt} + \vec{\omega}^\text{c}_\text{c} \times I^\text{c}_\text{c}\vec{\omega}^\text{c}_\text{c} = \sum_{i\in D}\left[\vec{M}^\text{c}_\text{i}\left(\frac{d\vec{\omega}^\text{c}_\text{c}}{dt}, \vec{V}^\text{c}_\text{c}, \vec{\omega}^\text{c}_\text{c}, \vec{\eta}^{\,\text{c}}, \delta_\text{r}, \delta_\text{l}\right) + \vec{r}^{\,\text{c}}_\text{i} \times \vec{F}^\text{c}_\text{i}\left(\frac{d\vec{V}^\text{c}_\text{c}}{dt}, \frac{d\vec{\omega}^\text{c}_\text{c}}{dt}, \vec{V}^\text{c}_\text{c}, \vec{\omega}^\text{c}_\text{c}, \vec{\eta}^{\,\text{c}}, \delta_\text{r}, \delta_\text{l}\right)\right], \tag{25}$$

with $\vec{M}_i^{\mathrm{c}}$ as a contributing moment within the index set of D. $\vec{r}_{\mathrm{i}}^{\,\mathrm{c}}$ is the corresponding position vector from the contribution to the CoM. The first contribution is the parafoil aerodynamic force ($\vec{F}_{\mathsf{p}_\mathrm{a}}^{\mathrm{c}}$) and moments ($\vec{M}_{\mathsf{p}_\mathrm{a}}^{\mathrm{c}}$) are defined as

$$\begin{aligned}
\vec{F}_{\mathsf{p}_\mathrm{a}}^{\mathrm{c}}(\vec{V}_{\mathrm{c}}^{\mathrm{c}}, \vec{\omega}_{\mathrm{c}}^{\mathrm{c}}, \vec{\eta}^{\,\mathrm{c}}, \delta_{\mathrm{r}}, \delta_{\mathrm{l}}) &= R(\mu)^\top \vec{F}_{\mathsf{p}_\mathrm{a}}^{\mathrm{p}}(\vec{V}_{\mathrm{p,air}}^{\mathrm{p}}, \vec{\omega}_{\mathrm{p}}^{\mathrm{p}}, \delta_{\mathrm{r}}, \delta_{\mathrm{l}}),\\
\vec{M}_{\mathsf{p}_\mathrm{a}}^{\mathrm{c}}(\vec{V}_{\mathrm{c}}^{\mathrm{c}}, \vec{\omega}_{\mathrm{c}}^{\mathrm{c}}, \vec{\eta}^{\,\mathrm{c}}, \delta_{\mathrm{r}}, \delta_{\mathrm{l}}) &= R(\mu)^\top \vec{M}_{\mathsf{p}_\mathrm{a}}^{\mathrm{p}}(\vec{V}_{\mathrm{p,air}}^{\mathrm{p}}, \vec{\omega}_{\mathrm{p}}^{\mathrm{p}}, \delta_{\mathrm{r}}, \delta_{\mathrm{l}}),\\
\vec{V}_{\mathrm{p,air}}^{\mathrm{p}} &= R(\mu)\left(\vec{V}_{\mathrm{c}}^{\mathrm{c}} - \vec{r}_{\mathsf{p}_\mathrm{a}}^{\,\mathrm{c}} \times \vec{\omega}_{\mathrm{c}}^{\mathrm{c}} + R(\vec{\eta}^{\,\mathrm{c}})\vec{V}_{\mathrm{w}}^{\mathrm{n}}\right),\\
\vec{\omega}_{\mathrm{p}}^{\mathrm{p}} &= R(\mu)\vec{\omega}_{\mathrm{c}}^{\mathrm{c}},
\end{aligned} \tag{26}$$

here $\vec{V}_{\mathrm{w}}^{\mathrm{n}}$ is the wind velocity vector. $\vec{F}_{\mathsf{p}_\mathrm{a}}^{\mathrm{p}}$ and $\vec{M}_{\mathsf{p}_\mathrm{a}}^{\mathrm{p}}$ are given in (6). The second contribution are load aerodynamics. The load aerodynamic force ($\vec{F}_{\mathsf{l}_\mathrm{a}}^{\mathrm{c}}$) and moments ($\vec{M}_{\mathsf{l}_\mathrm{a}}^{\mathrm{c}}$) are expressed similar as the parafoil aerodynamics as

$$\begin{aligned}
\vec{F}_{\mathsf{l}_\mathrm{a}}^{\mathrm{c}}(\vec{V}_{\mathrm{c}}^{\mathrm{c}}, \vec{\omega}_{\mathrm{c}}^{\mathrm{c}}, \vec{\eta}^{\,\mathrm{c}}) &= \vec{F}_{\mathsf{l}_\mathrm{a}}^{\mathrm{l}}(\vec{V}_{\mathrm{l,air}}^{\mathrm{l}}, \vec{\omega}_{\mathrm{l}}^{\mathrm{l}})\\
\vec{M}_{\mathsf{l}_\mathrm{a}}^{\mathrm{c}}(\vec{V}_{\mathrm{c}}^{\mathrm{c}}, \vec{\omega}_{\mathrm{c}}^{\mathrm{c}}, \vec{\eta}^{\,\mathrm{c}}) &= \vec{M}_{\mathsf{l}_\mathrm{a}}^{\mathrm{l}}(\vec{V}_{\mathrm{l,air}}^{\mathrm{l}}, \vec{\omega}_{\mathrm{l}}^{\mathrm{l}})\\
\vec{V}_{\mathrm{l,air}}^{\mathrm{l}} &= \vec{V}_{\mathrm{c}}^{\mathrm{c}} - \vec{r}_{\mathsf{l}_\mathrm{a}}^{\,\mathrm{l}} \times \vec{\omega}_{\mathrm{c}}^{\mathrm{c}} + R(\vec{\eta}^{\,\mathrm{c}})\vec{V}_{\mathrm{w}}^{\mathrm{n}}\\
\vec{\omega}_{\mathrm{l}}^{\mathrm{l}} &= \vec{\omega}_{\mathrm{c}}^{\mathrm{c}},
\end{aligned} \tag{27}$$

$\vec{F}_{\mathsf{l}_\mathrm{a}}^{\mathrm{l}}$ and $\vec{M}_{\mathsf{l}_\mathrm{a}}^{\mathrm{l}}$ are given in (7). The third contribution is the gravity force, which only works along the z_{n} axis of the world frame. The gravity force ($\vec{F}_{\mathsf{g}}^{\mathrm{c}}$) is modeled as

$$\vec{F}_{\mathsf{g}}^{\mathrm{c}}(\vec{\eta}^{\,\mathrm{c}}) = m_{\mathrm{c}} g \begin{bmatrix} -\sin(\theta^{\mathrm{c}}) \\ \sin(\phi^{\mathrm{c}})\cos(\theta^{\mathrm{c}}) \\ \cos(\phi^{\mathrm{c}})\cos(\theta^{\mathrm{c}}) \end{bmatrix}, \tag{28}$$

here g is the gravitational constant. The EoM (25) might have suggested that the gravity also has a moment contribution ($\vec{M}_{\mathrm{g}}^{\mathrm{c}}$). The gravity is a force acting in the CoM of the rigid body. Therefore, this component is absent and set to zero. The last contribution is the apparent mass. The apparent mass is expressed in the parafoil frame and is rotated from the parafoil frame to the $\{\mathrm{c}\}$ frame. The apparent mass force ($\vec{F}_{\mathsf{p}_\mathrm{m}}^{\mathrm{c}}$) and moment ($\vec{M}_{\mathsf{p}_\mathrm{m}}^{\mathrm{c}}$) are given as

$$\begin{aligned}
\vec{F}_{\mathsf{p}_\mathrm{m}}^{\mathrm{c}}\left(\frac{d\vec{V}_{\mathrm{c}}^{\mathrm{c}}}{dt}, \frac{d\vec{\omega}_{\mathrm{c}}^{\mathrm{c}}}{dt}, \vec{V}_{\mathrm{c}}^{\mathrm{c}}, \vec{\omega}_{\mathrm{c}}^{\mathrm{c}}, \vec{\eta}^{\,\mathrm{c}}\right) &= R(\mu)^\top \vec{F}_{\mathsf{p}_\mathrm{m}}^{\mathrm{p}}\left(\frac{d\vec{V}_{\mathrm{p,air}}^{\mathrm{p}}}{dt}, \vec{V}_{\mathrm{p,air}}^{\mathrm{p}}, \vec{\omega}_{\mathrm{p}}^{\mathrm{p}}\right),\\
\vec{M}_{\mathsf{p}_\mathrm{m}}^{\mathrm{c}}\left(\frac{d\vec{\omega}_{\mathrm{c}}^{\mathrm{c}}}{dt}, \vec{V}_{\mathrm{c}}^{\mathrm{c}}, \vec{\omega}_{\mathrm{c}}^{\mathrm{c}}, \vec{\eta}^{\,\mathrm{c}}\right) &= R(\mu)^\top \vec{M}_{\mathsf{p}_\mathrm{m}}^{\mathrm{p}}\left(\frac{d\vec{\omega}_{\mathrm{p}}^{\mathrm{p}}}{dt}, \vec{V}_{\mathrm{p,air}}^{\mathrm{p}}, \vec{\omega}_{\mathrm{p}}^{\mathrm{p}}\right),\\
\vec{V}_{\mathrm{p,air}}^{\mathrm{p}} &= R(\mu)(\vec{V}_{\mathrm{c}}^{\mathrm{c}} - \vec{r}_{\mathsf{p}_\mathrm{m}}^{\,\mathrm{c}} \times \vec{\omega}_{\mathrm{c}}^{\mathrm{c}} + R(\vec{\eta}^{\,\mathrm{c}})\vec{V}_{\mathrm{w}}^{\mathrm{n}}),\\
\frac{d\vec{V}_{\mathrm{p,air}}^{\mathrm{p}}}{dt} &= R(\mu)\left(\frac{d\vec{V}_{\mathrm{c}}^{\mathrm{c}}}{dt} - \vec{r}_{\mathsf{p}_\mathrm{m}}^{\,\mathrm{c}} \times \frac{d\vec{\omega}_{\mathrm{c}}^{\mathrm{c}}}{dt}\right),\\
\frac{d\vec{\omega}_{\mathrm{p}}^{\mathrm{p}}}{dt} &= R(\mu)\left(\frac{d\vec{\omega}_{\mathrm{c}}^{\mathrm{c}}}{dt}\right),
\end{aligned} \tag{29}$$

with $\vec{F}_{\mathsf{p}_\mathrm{m}}^{\mathrm{p}}$ and $\vec{M}_{\mathsf{p}_\mathrm{m}}^{\mathrm{p}}$ given in (14),(15) respectively.

3.6 Twelve DoF model model of PADS flight dynamics

The twelve DoF model is an extension of the six DoF model. Instead of looking at one rigid body, the parafoil and the SR or load will be considered as two separate rigid bodies. This makes some parts of the modeling easier. There is no need to combine the masses and inertia's in one mass and inertia in the CoM. There are two centers of mass, one for the parafoil and one for the load. The two rigid body should be contraint with respect to each other. Thi makes the modeling more complex. The tension lines allow for relative motion between the parafoil and the load. A tension line model is introduced to constrain the relative movement of the load w.r.t. the parafoil.

The index set of forces and moments D given for the 6 DoF model is separated in a set for the parafoil P and a set for the load L. P consists of the parafoil aerodynamics (p_a), the parafoil gravity (p_g), the parafoil apparent mass (p_m) and the parafoil tension line (p_t). This gives P as $\{\mathsf{p}_\mathrm{a}, \mathsf{p}_\mathrm{g}, \mathsf{p}_\mathrm{m}, \mathsf{p}_\mathrm{t}\}$. L consists of the load aerodynamics (l_a), the load gravity (l_g) and the load tension line (l_t). This gives L as $\{\mathsf{l}_\mathrm{a}, \mathsf{l}_\mathrm{g}, \mathsf{l}_\mathrm{t}\}$. Two sets of equations of motion are used to determine the motion of the parafoil and the load. The parafoil EoM are given as

$$m_\mathrm{p}\frac{d\vec{V}_\mathrm{p}^\mathrm{p}}{dt} + \vec{\omega}_\mathrm{p}^\mathrm{p} \times m_\mathrm{p}\vec{V}_\mathrm{p}^\mathrm{p} = \sum_{i\in P} \vec{F}_\mathrm{i}^\mathrm{p}\left(\frac{d\vec{V}_\mathrm{p}^\mathrm{p}}{dt}, \frac{d\vec{\omega}_\mathrm{p}^\mathrm{p}}{dt}, \vec{V}_\mathrm{p}^\mathrm{p}, \vec{\omega}_\mathrm{p}^\mathrm{p}, \vec{\eta}^{\,\mathrm{p}}, \delta_\mathrm{r}, \delta_\mathrm{l}\right) \tag{30}$$

and

$$I_\mathrm{p}^\mathrm{p}\frac{d\vec{\omega}_\mathrm{p}^\mathrm{p}}{dt} + \vec{\omega}_\mathrm{p}^\mathrm{p} \times I_\mathrm{p}^\mathrm{p}\vec{\omega}_\mathrm{p}^\mathrm{p} = \sum_{i\in P}\left[\vec{M}_\mathrm{i}^\mathrm{p}\left(\frac{d\vec{\omega}_\mathrm{p}^\mathrm{p}}{dt}, \vec{V}_\mathrm{p}^\mathrm{p}, \vec{\omega}_\mathrm{p}^\mathrm{p}, \vec{\eta}^{\,\mathrm{p}}, \delta_\mathrm{r}, \delta_\mathrm{l}\right) + \vec{r}_\mathrm{i}^{\,\mathrm{p}} \times \vec{F}_\mathrm{i}^\mathrm{p}\left(\frac{d\vec{V}_\mathrm{p}^\mathrm{p}}{dt}, \frac{d\vec{\omega}_\mathrm{p}^\mathrm{p}}{dt}, \vec{V}_\mathrm{p}^\mathrm{p}, \vec{\omega}_\mathrm{p}^\mathrm{p}, \vec{\eta}^{\,\mathrm{p}}, \delta_\mathrm{r}, \delta_\mathrm{l}\right)\right]. \tag{31}$$

$\vec{F}_\mathrm{i}^\mathrm{p}$ represents the different force contributions of P and $\vec{M}_\mathrm{i}^\mathrm{p}$ represents the different moment contributions of P. $\vec{r}_\mathrm{i}^{\,\mathrm{p}}$ is the corresponding position vector from the contribution to the parafoil CoM. $\vec{\eta}^{\,\mathrm{p}}$ is the parafoil orientation w.r.t. the world frame. The EoM for the load are

$$m_\mathrm{l}\frac{d\vec{V}_\mathrm{l}^\mathrm{l}}{dt} + \vec{\omega}_\mathrm{l}^\mathrm{l} \times m^\mathrm{l}\vec{V}_\mathrm{l}^\mathrm{l} = \sum_{i\in L} \vec{F}_\mathrm{i}^\mathrm{l}\left(\frac{d\vec{V}_\mathrm{l}^\mathrm{l}}{dt}, \frac{d\vec{\omega}_\mathrm{l}^\mathrm{l}}{dt}, \vec{V}_\mathrm{l}^\mathrm{l}, \vec{\omega}_\mathrm{l}^\mathrm{l}, \vec{\eta}^{\,\mathrm{l}}, \delta_\mathrm{r}, \delta_\mathrm{l}\right) \tag{32}$$

and

$$I_\mathrm{l}^\mathrm{l}\frac{d\vec{\omega}_\mathrm{l}^\mathrm{l}}{dt} + \vec{\omega}_\mathrm{l}^\mathrm{l} \times I_\mathrm{l}^\mathrm{l}\vec{\omega}_\mathrm{l}^\mathrm{l} = \sum_{i\in L}\left[\vec{M}_\mathrm{i}^\mathrm{l}\left(\frac{d\vec{\omega}_\mathrm{l}^\mathrm{l}}{dt}, \vec{V}_\mathrm{l}^\mathrm{l}, \vec{\omega}_\mathrm{l}^\mathrm{l}, \vec{\eta}^{\,\mathrm{l}}, \delta_\mathrm{r}, \delta_\mathrm{l}\right) + \vec{r}_\mathrm{i}^{\,\mathrm{l}} \times \vec{F}_\mathrm{i}^\mathrm{l}\left(\frac{d\vec{V}_\mathrm{l}^\mathrm{l}}{dt}, \frac{d\vec{\omega}_\mathrm{l}^\mathrm{l}}{dt}, \vec{V}_\mathrm{l}^\mathrm{l}, \vec{\omega}_\mathrm{l}^\mathrm{l}, \vec{\eta}^{\,\mathrm{l}}, \delta_\mathrm{r}, \delta_\mathrm{l}\right)\right]. \tag{33}$$

$\vec{F}_\mathrm{i}^\mathrm{l}$ represents the different force contributions of L and $\vec{M}_\mathrm{i}^\mathrm{l}$ represents the different moment contributions of L. $\vec{r}_\mathrm{i}^{\,\mathrm{l}}$ is the corresponding position vector from the contribution to the load CoM. $\vec{\eta}^{\,\mathrm{l}}$ is the load orientation w.r.t. the world frame. The aerodynamic contribution to the parafoil dynamics is expressed as

$$\begin{aligned}
\vec{F}_{\mathsf{p}_\mathrm{a}}^\mathrm{p}(\vec{V}_\mathrm{p}^\mathrm{p}, \vec{\omega}_\mathrm{p}^\mathrm{p}, \vec{\eta}^{\,\mathrm{p}}, \delta_\mathrm{r}, \delta_\mathrm{l}) &= \vec{F}_{\mathsf{p}_\mathrm{a}}^\mathrm{p}(\vec{V}_{\mathrm{p,air}}^\mathrm{p}, \vec{\omega}_\mathrm{p}^\mathrm{p}, \delta_\mathrm{r}, \delta_\mathrm{l}),\\
\vec{M}_{\mathsf{p}_\mathrm{a}}^\mathrm{p}(\vec{V}_\mathrm{p}^\mathrm{p}, \vec{\omega}_\mathrm{p}^\mathrm{p}, \vec{\eta}^{\,\mathrm{p}}, \delta_\mathrm{r}, \delta_\mathrm{l}) &= \vec{M}_{\mathsf{p}_\mathrm{a}}^\mathrm{p}(\vec{V}_{\mathrm{p,air}}^\mathrm{p}, \vec{\omega}_\mathrm{p}^\mathrm{p}, \delta_\mathrm{r}, \delta_\mathrm{l}), \qquad .\\
\vec{V}_{\mathrm{p,air}}^\mathrm{p} &= \vec{V}_\mathrm{p}^\mathrm{p} - \vec{r}_{\mathsf{p}_\mathrm{a}}^\mathrm{p} \times \vec{\omega}_\mathrm{p}^\mathrm{p} + R(\vec{\eta}^{\,\mathrm{p}})\vec{V}_\mathrm{w}^\mathrm{n}
\end{aligned} \tag{34}$$

$\vec{F}^{\mathrm{p}}_{\mathsf{p}_\mathrm{a}}$ and $\vec{M}^{\mathrm{p}}_{\mathsf{p}_\mathrm{a}}$ are given in (6). The aerodynamic contribution to the load is modeled as

$$\begin{aligned}
\vec{F}^{\mathrm{l}}_{\mathsf{l}_\mathrm{a}}(\vec{V}^{\mathrm{l}}_{\mathrm{l}}, \vec{\omega}^{\mathrm{l}}_{\mathrm{l}}) &= \vec{F}^{\mathrm{l}}_{\mathsf{l}_\mathrm{a}}(\vec{V}^{\mathrm{l}}_{\mathrm{l,air}}, \vec{\omega}^{\mathrm{l}}_{\mathrm{l}}),\\
\vec{M}^{\mathrm{l}}_{\mathsf{l}_\mathrm{a}}(\vec{V}^{\mathrm{l}}_{\mathrm{l}}, \vec{\omega}^{\mathrm{l}}_{\mathrm{l}}) &= \vec{M}^{\mathrm{l}}_{\mathsf{l}_\mathrm{a}}(\vec{V}^{\mathrm{l}}_{\mathrm{l,air}}, \vec{\omega}^{\mathrm{l}}_{\mathrm{l}}),\\
\vec{V}^{\mathrm{l}}_{\mathrm{l,air}} &= \vec{V}^{\mathrm{l}}_{\mathrm{l}} - \vec{r}^{\,\mathrm{l}}_{\mathrm{la}} \times \vec{\omega}^{\mathrm{l}}_{\mathrm{l}} + \vec{V}^{c}_{\mathrm{w}}.
\end{aligned} \tag{35}$$

with $\vec{F}^{\mathrm{l}}_{\mathsf{l}_\mathrm{a}}$ and $\vec{M}^{\mathrm{l}}_{\mathsf{l}_\mathrm{a}}$ are given in (7) The gravity force ($\vec{F}^{\mathrm{p}}_{\mathsf{p}_\mathrm{g}}$) of the parafoil is determined as

$$\vec{F}^{\mathrm{p}}_{\mathsf{p}_\mathrm{g}}(\vec{\eta}^{\,\mathrm{p}}) = m_{\mathrm{p}} g \begin{bmatrix} -\sin(\theta^{\mathrm{p}}) \\ \sin(\phi^{\mathrm{p}})\cos(\theta^{\mathrm{p}}) \\ \cos(\phi^{\mathrm{p}})\cos(\theta^{\mathrm{p}}) \end{bmatrix}, \tag{36}$$

the gravity force ($\vec{F}^{\mathrm{l}}_{\mathsf{l}_\mathrm{g}}$) of the load is

$$\vec{F}^{\mathrm{l}}_{\mathsf{l}_\mathrm{g}}(\vec{\eta}^{\,\mathrm{l}}) = m_{\mathrm{l}} g \begin{bmatrix} -\sin(\theta^{\mathrm{l}}) \\ \sin(\phi^{\mathrm{l}})\cos(\theta^{\mathrm{l}}) \\ \cos(\phi^{\mathrm{l}})\cos(\theta^{\mathrm{l}}) \end{bmatrix}. \tag{37}$$

The apparent mass force and moment are expressed as

$$\begin{aligned}
\vec{F}^{\mathrm{p}}_{\mathsf{p}_\mathrm{m}}\left(\frac{d\vec{V}^{\mathrm{p}}_{\mathrm{p}}}{dt}, \frac{d\vec{\omega}^{\mathrm{p}}_{\mathrm{p}}}{dt}, \vec{V}^{\mathrm{p}}_{\mathrm{p}}, \vec{\omega}^{\mathrm{p}}_{\mathrm{p}}, \vec{\eta}^{\,\mathrm{p}}\right) &= \vec{F}^{\mathrm{p}}_{\mathsf{p}_\mathrm{m}}\left(\frac{d\vec{V}^{\mathrm{p}}_{\mathrm{p,air}}}{dt}, \vec{V}^{\mathrm{p}}_{\mathrm{p,air}}, \vec{\omega}^{\mathrm{p}}_{\mathrm{p}}\right),\\
\vec{M}^{\mathrm{p}}_{\mathsf{p}_\mathrm{m}}\left(\frac{d\vec{\omega}^{\mathrm{p}}_{\mathrm{p}}}{dt}, \vec{V}^{\mathrm{p}}_{\mathrm{p}}, \vec{\omega}^{\mathrm{p}}_{\mathrm{p}}, \vec{\eta}^{\,\mathrm{p}}\right) &= \vec{M}^{\mathrm{p}}_{\mathsf{p}_\mathrm{m}}\left(\frac{d\vec{\omega}^{\mathrm{p}}_{\mathrm{p}}}{dt}, \vec{V}^{\mathrm{p}}_{\mathrm{p,air}}, \vec{\omega}^{\mathrm{p}}_{\mathrm{p}}\right),\\
\vec{V}^{\mathrm{p}}_{\mathrm{p,air}} &= \vec{V}^{\mathrm{p}}_{\mathrm{p}} - \vec{r}^{\,\mathrm{p}}_{\mathsf{p}_\mathrm{m}} \times \vec{\omega}^{\mathrm{p}}_{\mathrm{p}} + R(\vec{\eta}^{\,\mathrm{p}})\vec{V}^{\mathrm{n}}_{\mathrm{w}},\\
\frac{d\vec{V}^{\mathrm{p}}_{\mathrm{p,air}}}{dt} &= \frac{d\vec{V}^{\mathrm{p}}_{\mathrm{p}}}{dt} - \vec{r}^{\,\mathrm{p}}_{\mathsf{p}_\mathrm{m}} \times \frac{d\vec{\omega}^{\mathrm{p}}_{\mathrm{p}}}{dt},
\end{aligned} \tag{38}$$

with $\vec{F}^{\mathrm{p}}_{\mathsf{p}_\mathrm{m}}$ and $\vec{M}^{\mathrm{p}}_{\mathsf{p}_\mathrm{m}}$ given in (14),(15) respectively. The parafoil tension line forces and moments are

$$\begin{aligned}
\vec{F}^{\mathrm{p}}_{\mathsf{p}_\mathrm{t}}(\vec{r}^{\,\mathrm{p}}_{\mathrm{p}}, \vec{r}^{\,\mathrm{p}}_{\mathrm{l}}, \vec{\eta}^{\,\mathrm{p}}, \vec{\eta}^{\,\mathrm{l}}, \vec{V}^{\mathrm{p}}_{\mathrm{p}}, \vec{V}^{\mathrm{l}}_{\mathrm{l}}, \vec{\omega}^{\mathrm{p}}_{\mathrm{p}}) &= \vec{F}^{\mathrm{p}}_{\mathsf{p}_\mathrm{t}}\left(\vec{r}^{\,\mathrm{p}}_{\mathrm{t}}, \frac{d\vec{r}^{\,\mathrm{p}}_{\mathrm{t}}}{dt}\right),\\
\vec{M}^{\mathrm{p}}_{\mathsf{p}_\mathrm{t}}(\vec{\eta}^{\,\mathrm{p}}, \vec{\eta}^{\,\mathrm{l}}, \vec{\omega}^{\mathrm{p}}_{\mathrm{p}}, \vec{\omega}^{\mathrm{l}}_{\mathrm{l}}) &= \vec{M}^{\mathrm{p}}_{\mathsf{p}_\mathrm{t}}\left(\vec{\eta}^{\,\mathrm{t}}, \frac{d\vec{\eta}^{\,\mathrm{t}}}{dt}\right),\\
\vec{r}^{\,\mathrm{p}}_{\mathrm{t}} &= R(\vec{\eta}^{\,\mathrm{p}})(\vec{r}^{\,\mathrm{n}}_{\mathrm{p}} - \vec{r}^{\,\mathrm{n}}_{\mathrm{l}}),\\
\vec{\eta}^{\,\mathrm{t}} &= \vec{\eta}^{\,\mathrm{p}} - \vec{\eta}^{\,\mathrm{l}}\\
\frac{d\vec{r}^{\,\mathrm{p}}_{\mathrm{t}}}{dt} &= \vec{r}^{\,\mathrm{p}}_{\mathrm{t}} \times \omega^{\mathrm{p}}_{\mathrm{p}} + \vec{V}^{\mathrm{p}}_{\mathrm{p}} - R(\vec{\eta}^{\,\mathrm{t}})\vec{V}^{\,\mathrm{l}}_{\mathrm{l}}\\
\frac{d\vec{\eta}^{\,\mathrm{t}}}{dt} &= J(\vec{\eta}^{\,\mathrm{p}})\vec{\omega}^{\mathrm{p}}_{\mathrm{p}} - J(\vec{\eta}^{\,\mathrm{l}})\vec{\omega}^{\mathrm{l}}_{\mathrm{l}},
\end{aligned} \tag{39}$$

$\vec{r}^{\,\mathrm{n}}_{\mathrm{p}}$ is the position vector of the parafoil defined in the world frame. Similar $\vec{r}^{\,\mathrm{n}}_{\mathrm{l}}$ is the position vector of the load defined in the world frame. $\vec{F}^{\mathrm{p}}_{\mathsf{p}_\mathrm{t}}$ and $\vec{M}^{\mathrm{p}}_{\mathsf{p}_\mathrm{t}}$ are given in (19). The load tension line force and moments are

$$\begin{aligned}
\vec{F}^{\mathrm{l}}_{\mathsf{l}_\mathrm{t}}(\vec{r}^{\,\mathrm{p}}_{\mathrm{p}}, \vec{r}^{\,\mathrm{p}}_{\mathrm{l}}, \vec{\eta}^{\,\mathrm{p}}, \vec{\eta}^{\,\mathrm{l}}, \vec{V}^{\mathrm{p}}_{\mathrm{p}}, \vec{V}^{\mathrm{l}}_{\mathrm{l}}, \vec{\omega}^{\mathrm{p}}_{\mathrm{p}}) &= \vec{F}^{\mathrm{l}}_{\mathsf{l}_\mathrm{t}}\left(\vec{r}^{\,\mathrm{p}}_{\mathrm{t}}, \vec{\eta}^{\,\mathrm{t}}, \frac{d\vec{r}^{\,\mathrm{p}}_{\mathrm{t}}}{dt}\right)\\
\vec{M}^{\mathrm{l}}_{\mathsf{l}_\mathrm{t}}(\vec{\eta}^{\,\mathrm{p}}, \vec{\eta}^{\,\mathrm{l}}, \vec{\omega}^{\mathrm{p}}_{\mathrm{p}}, \vec{\omega}^{\mathrm{l}}_{\mathrm{l}}) &= \vec{M}^{\mathrm{l}}_{\mathsf{l}_\mathrm{t}}\left(\vec{\eta}^{\,\mathrm{t}}, \frac{d\vec{\eta}^{\,\mathrm{t}}}{dt}\right)
\end{aligned}. \tag{40}$$

with $\vec{F}^{\mathrm{l}}_{\mathsf{l}_\mathrm{t}}$ and $\vec{M}^{\mathrm{l}}_{\mathsf{l}_\mathrm{t}}$ given in (20).

3.7 Additional descriptions of dynamic effects

In this report one more involved aerodynamic model and one more complex tension line model are explored. First the aerodynamic model is explained. The parafoil can be divided in multiple panels. The panels can rotate w.r.t. each other, resulting in a flexible representation of the parafoil. The aerodynamic force is then also expressed as a force per panel, instead of one aerodynamic force for the whole parafoil. In [4] an aerodynamic expression is derived for the aerodynamic force ($\vec{F}^{\mathrm{p}}_{\mathsf{p}_\mathrm{a},i}$) per panel as

$$\begin{aligned}\vec{F}^{\mathrm{p}}_{\mathsf{p}_\mathrm{a},\mathrm{i}}(\vec{V}^{\mathrm{i}}_{\mathrm{i,air}},\delta_\mathrm{i}) = \frac{1}{2}\rho S_\mathrm{i}\Bigg(&C_{\mathrm{L}\delta_\mathrm{i}}\sqrt{(u^{\mathrm{i}}_{\mathrm{i,air}})^2+(w^{\mathrm{i}}_{\mathrm{i,air}})^2}\begin{bmatrix} w^{\mathrm{i}}_{\mathrm{i,air}} \\ 0 \\ -u^{\mathrm{i}}_{\mathrm{i,air}}\end{bmatrix} + \\ &C_{\mathrm{D}\delta_\mathrm{i}}\sqrt{(u^{\mathrm{i}}_{\mathrm{i,air}})^2+(v^{\mathrm{i}}_{\mathrm{i,air}})^2+(w^{\mathrm{i}}_{\mathrm{i,air}})^2}\begin{bmatrix} u^{\mathrm{i}}_{\mathrm{i,air}} \\ v^{\mathrm{i}}_{\mathrm{i,air}} \\ w^{\mathrm{i}}_{\mathrm{i,air}}\end{bmatrix}\Bigg),\end{aligned} \tag{41}$$

with $\vec{V}^{\mathrm{i}}_{\mathrm{i,air}}$ as the air velocity of the panel, δ_i as the deflection of the panel, S_i as the aerodynamic reference area of the panel. $C_{\mathrm{L}\delta_\mathrm{i}}$ and $C_{\mathrm{D}\delta_\mathrm{i}}$ are the aerodynamic lift and drag coefficient of the panel, dependent on δ_i. The resulting force can be modeled on each panel. The total resulting aerodynamic moments ($\vec{M}^{\mathrm{p}}_{\mathsf{p}_\mathrm{a}}$) is

$$\vec{M}^{\mathrm{p}}_{\mathsf{p}_\mathrm{a}}(\vec{V}^{\mathrm{i}}_{i,\mathrm{air}},\delta_i,\vec{r}^{\,\mathrm{p}}_i,\vec{\eta}^{\,\mathrm{i}}) = \sum_i^N\left(\vec{r}^{\,\mathrm{p}}_i \times R(\vec{\eta}^{\,\mathrm{i}})\vec{F}^{\mathrm{p}}_{\mathsf{p}_\mathrm{a},i}(\vec{V}^{\mathrm{i}}_{i,\mathrm{air}},\delta_i)\right), \tag{42}$$

here N is the amount of panels. $\vec{r}^{\,\mathrm{p}}_\mathrm{i}$ is the position vector from the parafoil CoM to the panel and $\vec{\eta}^{\,\mathrm{i}}$ is the orentation of the panel w.r.t. the parafoil. Since in this report the parafoil is considered as one rigid body, this aerodynamic expression reduces to the expression given in (6). Therefore, this expression is not implemented.

The tension line model given in (19) is a simplistic model. A general PADS consists of tens of tension lines, instead of just one. The moments due to the tension lines are in reality a result of the tension line forces, instead of a torsion stiffness and damping. Multiple tension line forces are then modeled between the attachment points of the parafoil and the load. [13] and [22] use a similar approach. The tension lines between the parafoil and the payload are modeled as multiple 1D spring-damper systems, which are only able to handle load in one direction and only if the line is stretched. compressing the line is not realistic, thus creating a nonlinear model. The tension force (F_t) is expressed as

$$F_\mathrm{t} = -k(l-l_\mathrm{eq}) - d\dot{l} \tag{43}$$

with l being the length of the line, l_eq as the equilibrium length, k is the spring constant and d is the damping constant. In a three dimensional space it is assumed that the force directly counteracts the excitation. Only the velocity is damped, which is inline with the excitation. This results in a tension force ($\vec{F}^{\mathrm{p}}_\mathrm{t}$) in one of the load attachments points as

$$\vec{F}^{\mathrm{l}}_\mathrm{t} = -k\vec{r}^{\,\mathrm{l}}_\mathrm{t}\left(1-\frac{l_\mathrm{eq}}{||\vec{r}^{\,\mathrm{l}}_\mathrm{t}||_2}\right) - d\left(\frac{\dot{\vec{r}}^{\,\mathrm{l}\top}_\mathrm{t}\vec{r}^{\,\mathrm{l}}_\mathrm{t}}{\vec{r}^{\,\mathrm{l}\top}_\mathrm{t}\vec{r}^{\,\mathrm{l}}_\mathrm{t}}\right)\vec{r}^{\,\mathrm{l}}_\mathrm{t}. \tag{44}$$

The length l is replaced with the position vector from the attachment point on the parafoil to the attachment point on the load ($\vec{r}_{\mathrm{t}}^{\,\mathrm{l}}$). The line force only works if $||\vec{r}_{\mathrm{t}}^{\,\mathrm{l}}||_2 > l_{\mathrm{eq}}$. By modeling multiple lines between multiple attachments point, the tension moments follow as a result of the tension forces.

3.8 Model Composition

By embedding all the forces and moments in the EoM and rearranging terms the 6 DoF model can be written as a nonlinear model. The model is based on the vectors $\zeta = [\vec{V}_{\mathrm{c}}^{\,\mathrm{c}\top} \quad \vec{\omega}_{\mathrm{c}}^{\,\mathrm{c}\top}]^\top$, $\xi = [\vec{r}_{\mathrm{c}}^{\,\mathrm{n}\top} \quad \vec{\eta}^{\,\mathrm{c}\top}]^\top$, δ is the left and right deflection (δ_{l} & δ_{r}). w is the disturbance, which is the wind velocity ($\vec{V}_{\mathrm{w}}^{\,\mathrm{n}}$). The model is

$$M\dot{\zeta} = C_\zeta(\zeta)\zeta + C_w(\zeta, \xi, w) + D(\zeta, \xi, \delta, w) + G(\xi) \tag{45}$$

with M as the mass matrix with the mass, inertia and the apparent mass. $C_\zeta(\zeta)$ embeds al terms related to the EoM and apparent mass based on the vector ζ. $C_w(\zeta, \xi, w)$ embeds the remaining terms of the apparent mass. They become zero if the wind disturbance is not present. $D(\zeta, \xi, \delta, w)$ are all the aerodynamic terms and $G(\xi)$ is the gravity. ζ and ξ are related through

$$\dot{\xi} = \underbrace{\begin{bmatrix} R(\vec{\eta}^{\,\mathrm{c}})^\top & 0 \\ 0 & T(\vec{\eta}^{\,\mathrm{c}}) \end{bmatrix}}_{J} \zeta. \tag{46}$$

By defining the state vector as $[x_1^\top \quad x_2^\top]^\top = [\zeta^\top \quad \xi^\top]^\top$ a state space is constructed as

$$\dot{x} = f(x, u, w) = \begin{bmatrix} 0 & J(x_1) \\ 0 & M^{-1}C_\zeta(x_2) \end{bmatrix} x + \begin{bmatrix} 0 \\ M^{-1}\left[C_w(x_1, x_2, w) + D(x_1, x_2, u, w) + G(x_1)\right] \end{bmatrix} \tag{47}$$

The inputs are the parafoil left and right deflection. This gives $u = \delta$. w is the disturbance and is still defined as the wind velocity ($\vec{V}_{\mathrm{w}}^{\,\mathrm{n}}$). Four outputs of interest are defined. The first is the heading angle, also presented as ψ, the second is the turning rate defined as $\dot{\psi}$. The third and fourth are the vertical and horizontal velocities of the load, defined in the world frame. The output is defined as

$$y = h(x) = \begin{bmatrix} \psi^{\mathrm{l}} \\ \dot{\psi}^{\mathrm{l}} \\ V_{\mathrm{h}}^{\mathrm{n}} \\ V_{\mathrm{v}}^{\mathrm{n}} \end{bmatrix} = \begin{bmatrix} \psi^{\mathrm{l}} \\ \dot{\psi}^{\mathrm{l}} \\ \sqrt{(u_{\mathrm{l}}^{\mathrm{n}})^2 + (v_{\mathrm{l}}^{\mathrm{n}})^2} \\ w_{\mathrm{l}}^{\mathrm{n}} \end{bmatrix} \tag{48}$$

with

$$\begin{aligned} \vec{\eta}^{\,\mathrm{l}} &= \vec{\eta}^{\,\mathrm{c}}, \\ \dot{\vec{\eta}}^{\,\mathrm{l}} &= J(\vec{\eta}^{\,\mathrm{l}})\vec{\omega}_{\mathrm{l}}^{\mathrm{l}}, \\ \vec{V}_{\mathrm{l}}^{\mathrm{n}} &= R^\top(\vec{\eta}^{\,\mathrm{l}})\left(\vec{V}_{\mathrm{c}}^{\mathrm{c}} - \vec{r}_{\mathrm{l}}^{\,\mathrm{l}} \times \vec{\omega}_{\mathrm{c}}^{\mathrm{c}}\right). \end{aligned} \tag{49}$$

The 12 DoF model is written similar as (45). The vector ζ becomes $[\vec{V}_{\mathrm{p}}^{\,\mathrm{p}\top} \quad \vec{V}_{\mathrm{l}}^{\,\mathrm{l}\top} \quad \vec{\omega}_{\mathrm{p}}^{\,\mathrm{p}\top} \quad \vec{\omega}_{\mathrm{l}}^{\,\mathrm{l}\top}]^\top$ and ξ becomes $[\vec{r}_{\mathrm{p}}^{\,\mathrm{n}\top} \quad \vec{r}_{\mathrm{l}}^{\,\mathrm{n}\top} \quad \vec{\eta}^{\,\mathrm{p}\top} \quad \vec{\eta}^{\,\mathrm{l}\top}]^\top$. The tension force is added in the matrices $C_\xi(\xi)$, $D_\zeta(\xi)$ and S. The system is expressed as

$$M\dot{\zeta} = C_\zeta(\zeta)\zeta + C_w(\zeta, \xi, w) + C_\xi(\xi)\xi + D_\zeta(\xi)\zeta + D(\zeta, \xi, \delta, w) + G(\xi) + S. \tag{50}$$

The vector ξ and ζ are related through

$$\dot{\xi} = \underbrace{\begin{bmatrix} R(\vec{\eta}^{\,\mathrm{p}})^\top & 0 & 0 & 0 \\ 0 & R(\vec{\eta}^{\,\mathrm{l}})^\top & 0 & 0 \\ 0 & 0 & T(\vec{\eta}^{\,\mathrm{p}}) & 0 \\ 0 & 0 & 0 & T(\vec{\eta}^{\,\mathrm{l}}) \end{bmatrix}}_{J} \zeta. \tag{51}$$

The state vector for the 12 DoF model is $[x_1^\top \quad x_2^\top]^\top = [\zeta^\top \quad \xi^\top]^\top$. The state space model is almost similar to the one constructed in (63) for the 6 DoF model and by adding the tension force results in

$$\begin{aligned} \dot{x} = f(x,u,w) = \begin{bmatrix} 0 & J(x_1) \\ M^{-1}C_\xi(x_1) & M^{-1}[C_\zeta(x_2) + D_\zeta(x_1)] \end{bmatrix} x + \\ \begin{bmatrix} 0 \\ M^{-1}\left[C_w(x_1,x_2,w) + D(x_1,x_2,u,w) + G(x_1) + S\right] \end{bmatrix} \end{aligned} \tag{52}$$

The outputs are defined as the heading of the load (ψ^{l}), the turning rate of the the load ($\dot{\psi}^{\mathrm{l}}$) and the vertical and horizontal velocity of the load as defined in the output of the 6 DoF model as

$$y = h(x) = \begin{bmatrix} \psi^{\mathrm{l}} \\ \dot{\psi}^{\mathrm{l}} \\ V_{\mathrm{h}}^{\mathrm{n}} \\ V_{\mathrm{v}}^{\mathrm{n}} \end{bmatrix} = \begin{bmatrix} \psi^{\mathrm{l}} \\ \dot{\psi}^{\mathrm{l}} \\ \sqrt{(u_{\mathrm{l}}^{\mathrm{n}})^2 + (v_{\mathrm{l}}^{\mathrm{n}})^2} \\ w_{\mathrm{l}}^{\mathrm{n}} \end{bmatrix} \tag{53}$$

with

$$\vec{V}_{\mathrm{l}}^{\mathrm{n}} = R^\top(\vec{\eta}^{\,\mathrm{l}})\vec{V}_{\mathrm{l}}^{\mathrm{l}}. \tag{54}$$

4 Implementation and Simulation

The proposed models are implemented in MATLAB and SIMULINK. Both the 6 DoF model and the 12 DoF model are implemented, such that it is possible to enable and disable the contributions to the model. The added added effect of the contributions can be compared. The contributions which can be enabled and disabled are the gravity, the parafoil aerodynamics, the load aerodynamics and the apparent mass. Sec. 4.1 will show the SIMULINK implementation and Sec. 4.2 and 4.3 show the simulation results. Two videos are created with Simscape. One shows the simulation result of the 6 DoF model and the other video shows the same simulation for the 12 DoF model. They are found at `https://youtu.be/vr0LlCARQw4` and `https://youtu.be/CT686KLwrkk`.

4.1 Simulink model

Both the 6 DoF and the 12 DoF have a similar implementation. Therefore, only the 12 DoF SIMULINK model will be discussed. The model overview is shown in Figure 4 The model consists of 5 part:

- Input
- Wind model
- Simscape model
- Forces and Moments
- Model data
- Output data

The Input consists of the input variables of the model. In this case the left and right deflection are given as an vector based on a time vector. The wind model determines the wind velocity vector in the position of the parafoil and the load. A simple wind model is implemented. The wind velocity is only based on the position in the world frame. The Simscape model, is based on the Simscape multibody library and captures the motion of the parafoil and the load, based on the masses, inertias, input forces and input moments. The gravity is also part of the Simscape model and the tension line between the parafoil and load is modeled with a Simscape Cartesian joint and a gimbal joint with internal spring-damper dynamics. In the Simscape models all the needed states are measured. The measure states can be viewed in the model data section. The forces and moments determine the aerodynamic forces and moments and the apparent mass force and moment based on the measured states. In the section a corresponding MATLAB model is called, which calculates the forces and moments, corresponding with the presented equation in Section 3. The output data determines the specific defined outputs of the model.

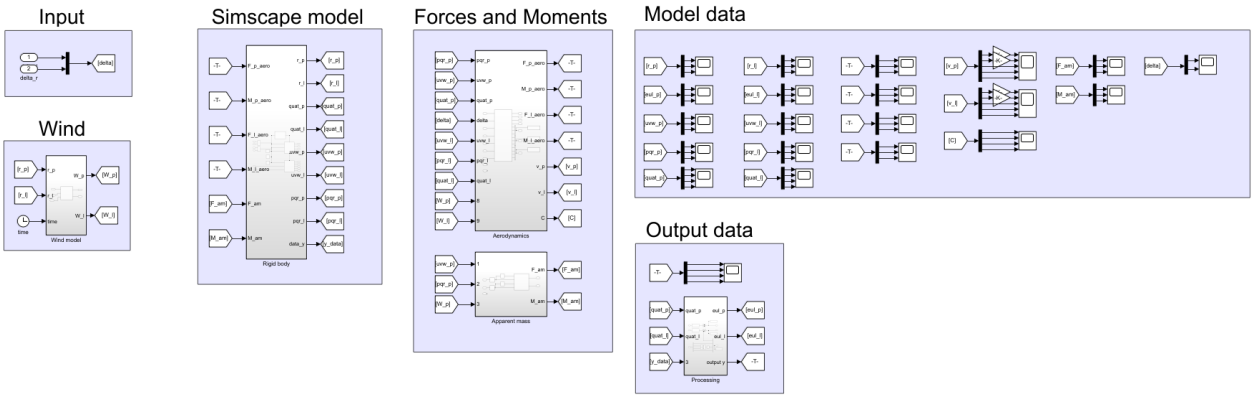

Figure 4: 12 DoF Simulink model, overview

To elaborate a bit on the used Simscape library. Figure 5 shows the implementation of the parafoil. The parafoil frame is connected through a 6 DoF joint to the world frame. On the side of the parafoil frame, a mass block is connected including the parafoil mass and inertia, a visualization file is connected and an external force and moments block is connected. The sensors are connected between the world frame and the parafoil frame measuring the position and orientation of the parafoil frame with respect of the world frame and the body velocity and body angular velocity in the parafoil frame. The measured state are connected the output of the SIMULINK block and also send to the MATLAB workspace.

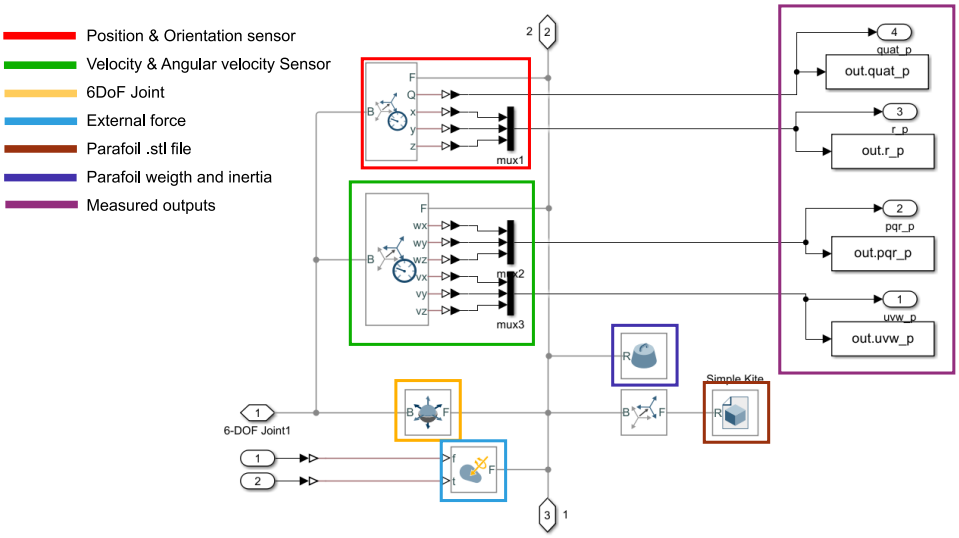

Figure 5: Simscape - parafoil model

The Simulink model can be called from MATLAB as following. The simulation folder contains the sub-folders 'models', with the models of the SR and 'functions' with all the needed MATLAB function to run the model. The parameter file can also be found in this folder. These folders are added to the MATLAB path. As following a struct `Enable` is defined, enabling the model contri-

butions. additionally, `Enable.W` enables the wind model. `Enable.Database` enables a look-up table for the aerodynamic coefficient otherwise a linear model is used. `Enable.Interp` enables linear interpolation between the coefficients in the aerodynamic look-up table. As following the system parameters are loaded. The input vector is created based on a time vector and the state vector at $t = 0$ is defined. As last the SIMULINK model is called and the simulation results are loaded in MATLAB. In MATLAB code this looks like

```
%% Add to path
addpath([currentFolder,'\function'])
addpath([currentFolder,'\models'])

%% System mode
Enable.F_g      = true;
Enable.P_aero   = true;
Enable.L_aero   = true;
Enable.AM       = true;
Enable.W        = true;
Enable.Interp   = true;
Enable.Database = 1;

%% Load system parameters
[Sys.Env,Sys.CoM,Sys.Para,Sys.Load,Sys.Lines] = Sys_Parameters(Enable);
Sys.Env.W = [0;0;0]; %wind velocity vector

%% Simulations
t.step = 1e-3;
t.end = 40;
t.span = 0:t.step:t.end;
Δ = 0*ones(length(t.span),2);
input = [t.span' Δ];

%% x0 state vector
TW.x0 = zeros(28,1);
TW.x0(4:6) = -Sys.Lines.r;
TW.x0(7:9) = [0 0 0]';
TW.x0(13:15) = [1;0;0];
TW.x0(16:18) = [1;0;0];
TW.x0(25:27) = Sys.Lines.r;

%% Call Simulink
in = Simulink.SimulationInput('Twelve_DoF_simscape_model_joint');
in=in.setExternalInput(input);
Sl_TW.out=sim(in);
```

4.2 Steady state model behavior

With the SIMULINK model it is possible to make simulations and analyze the behavior of the constructed models. First the steady state flight behavior will be analyzed for the 6 DoF model and the 12 DoF model. Next, the dynamic behavior is analyzed. When the PADS is dropped from a height, the system will converge to steady state motion. The velocity and the angular velocity of the model become constant as long as the model is not disturbed by disturbances or a change in the control inputs. For each constant control input the model converges to a different steady-state point. The steady state motion of the model can be found as equilibrium points of the body velocity and the body angular velocity. The EoM should be solved, such that the derivatives of the body velocity and angular velocity are zero. The corresponding velocity and

angular velocity is the equilibrium point. A constant pitch and roll angle are also included. The model dynamics are dependent on those. For each equilibrium point there is a corresponding constant control input. The equilibrium point and the corresponding control input always come in pairs. Solving the system for these equilibrium points is difficult, due to the complexity of the aerodynamic forces, but the attractive equilibrium points can be found by means of simulation or a successive root-finding algorithm, like the Newton–Raphson method. The parameter set given in [21] is used for simulation, since the set of parameters is all most complete and the paper presents results with which later on the model can be compared with. Since landing the load/SR is of interest, the flight behavior from the loads point of view is analyzed, thus when is referred to the velocity, angles or angular velocity, the corresponding state of the load in the load frame is meant.

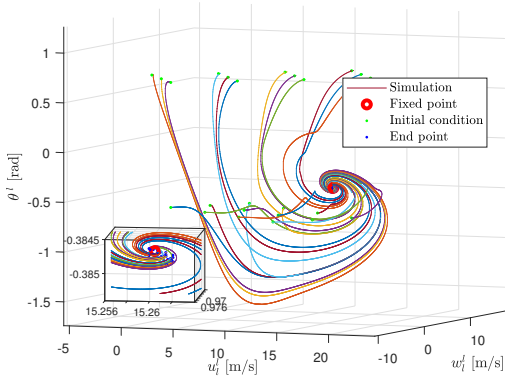

Figure 6: Convergence for $\delta_s = 0$

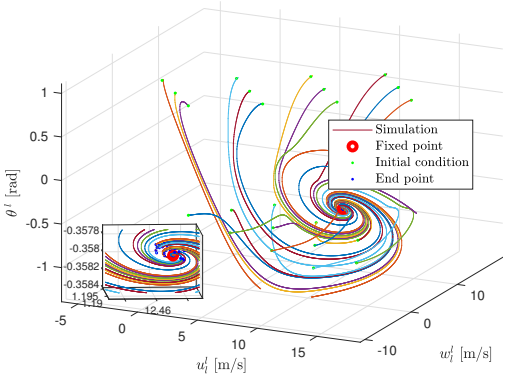

Figure 7: Convergence for $\delta_s = 0.5$

When simulating the system with a constant control input, The velocity component $\vec{v}_l^{\,l}$ converges to zero, as well as the angular velocity ($\vec{\omega}_l^{\,l}$) and the roll angle (ϕ^l). The yaw angle (ψ^l) can be any constant value. The velocity components u_l^l and w_l^l and the angle θ^l converge to a steady state, as is shown in Figure 6. and 7. These are of interest to find the equilibrium point. By substituting the known values in the EoM of both models, the system can be reduced to a force and moment balance between the aerodynamic forces and moments and the gravity force. Solving the system analytically is complex due to the expressions of the aerodynamics. It is possible to determine a local Jacobian of the system, but this takes up to a couple of minutes. This is too slow to use in an successive algorithm. Therefore, the Broyden's method is used to find state velocities and angles. Figure 6 shows multiple simulations from different initial conditions together with the approximated equilibrium point for zero control deflections. The figure shows all simulations converging to the same point of steady state motion. Broyden's method gives the same equilibrium point. Figure 7 shows similar results for a constant symmetric deflection of 0.5. The resulting equilibrium point is determined for each constant symmetric deflection as shown in Figure 8. The figures show the ability of the parafoil to brake its forward velocity (u_l^l) by 3.5 [m/s]. It increases its downward velocity slightly (u_l^l) by 0.3 [m/s]. The apparent mass effect decreases the forward velocity by 1.5 [m/s] and increases the downward velocity with 0.2 [m/s]. It increases the pitch (θ^l) with 0.11 [rad]. The 6 DoF model and the 12 DoF model do not show differences significant to the flight dynamics.

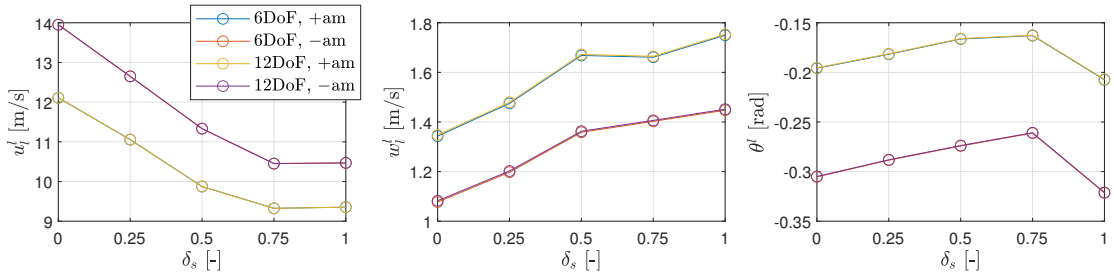

Figure 8: Steady state flight behavior for δ_s

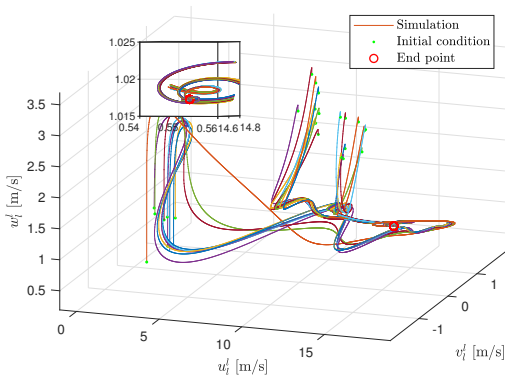

Figure 9: Convergence $\vec{V}_1^1$ for $\delta_a = 0.5$

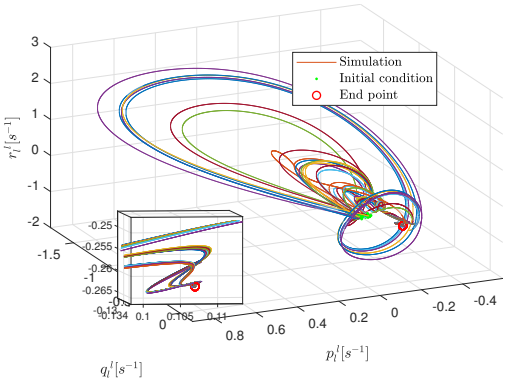

Figure 10: Convergence $\vec{\omega}_1^1$ for $\delta_a = 0.5$

The same analysis can be done for constant asymmetrical deflections as input. The right deflection is kept at zero. The left deflection is varied from 0 to 1. The simulations show that the system reaches a steady state motion, with a steady state velocity, angular velocity and a steady state pitching and rolling angle. The yaw angle does not converge. To find the equilibrium point, the system should be solved for all derivatives being zero with exception of the yaw rate and the position. Since Brodyen's method is unable to converge, the equilibrium point is determined based on the simulations. Figure 9 and 10 show the velocity and angular velocity converging to a single point for 0.5 asymmetric deflection. The same figures can be made for other asymmetric deflections.

Figure 11 and 12 show the equilibrium points for the velocity and the angular velocity versus a constant asymmetric deflection. The forward velocity increases between 1 and 2 [m/s] with an asymmetric deflection varying from .25 to 1. The side velocity (v_1^1) increases with 1 [m/s] from .25 to 1 asymmetric deflection. The downwards velocity decreases with 0.2 [m/s] for the 6 DoF and 0.4 [m/s] for the 12 DoF model. The angular velocity p_1^1 decreases from -0.02 [s^{-1}] for δ_a is 0.25 to -0.3 [s^{-1}] for δ_a is 1. r_1^1). q_1^1) increases from 0.02 [s^{-1}] to 0.3-0.45 [s^{-1}]. r_1^1 decreases with -0.3 [s^{-1}]. The roll angle decreases from -0.1 [rad] to -0.65 [rad]. the pitch angle decreases to -0.3 [rad] to -0.55 [rad]. The apparent mass effect gives a clear difference in all velocities, angular velocities and body angles. Moreover, the figures show divergences between the 6 DoF model and 12 DoF model. Especially the downwards velocity diverges with 0.2 [m/s] difference for $\delta_a = 1$. This differences could be caused by a small relative roll and pitch angle between the parafoil and the load.

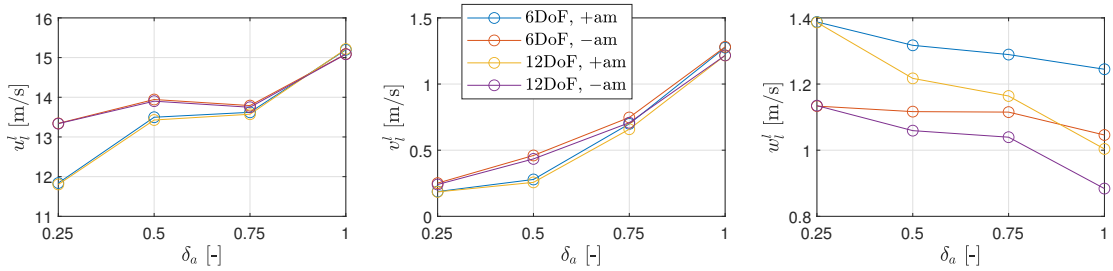

Figure 11: Steady state flight behavior $\delta_a \rightarrow \vec{V}_1^1$

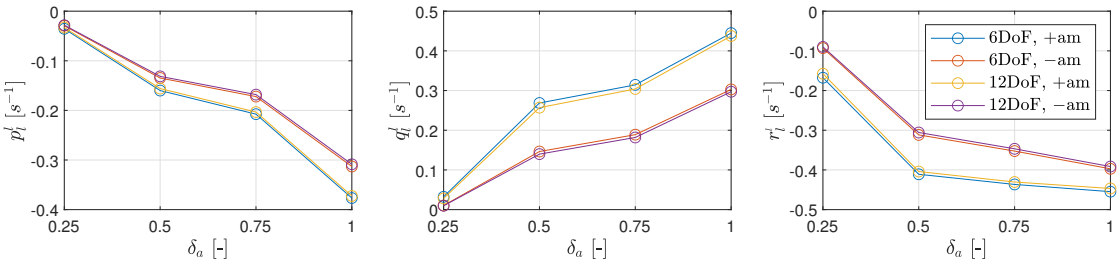

Figure 12: Steady state flight behavior $\delta_a \rightarrow \vec{\omega}_1^1$

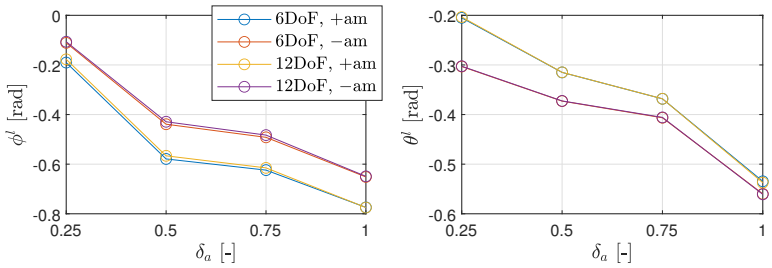

Figure 13: Steady state flight behavior $\delta_a \rightarrow \vec{\eta}^1$

4.3 Dynamic model behavior

To analyze the dynamic flight behavior, the system in steady state is disturbed by changing the control deflection from zero to either a symmetric or an asymmetric deflection. Figure 14 shows the dynamic behavior of the forward velocity and the downward velocity and the pitch for a symmetric deflection of 0.25 and 0.75. The forward velocity gives a rise time of 2 [s], a settling time of 7.5 [s] and a relative overshoot of 0.33 [-]. The apparent mass adds a steady state offset in the flight behavior. It does not seem to affect the dynamic flight behavior. The 6 DoF and 12 DoF model do not show differences. The downwards velocity has a rise time of 0.2 [s] and a settling time of 4 [s] and a relative overshoot of 0.2 [-]. The 12 DoF model shows some additional oscillations due to the spring damper connecting the parafoil and the load. The 12 DoF model

has a rise time of 0.05 [s] and a settling time of 5 [s] and a relative overshoot of 2.3 [-]. The apparent mass only shifts the behavior. The pitch θ^{l} oscillates with a rise time of 0.1 [s], but a settling time of over 15 [s]. The relative overshoot is 0.3 [-]. Moreover, the apparent mass only adds a steady state shift. The 12 DoF does not show additional flight behavior w.r.t. the 6 DoF model.

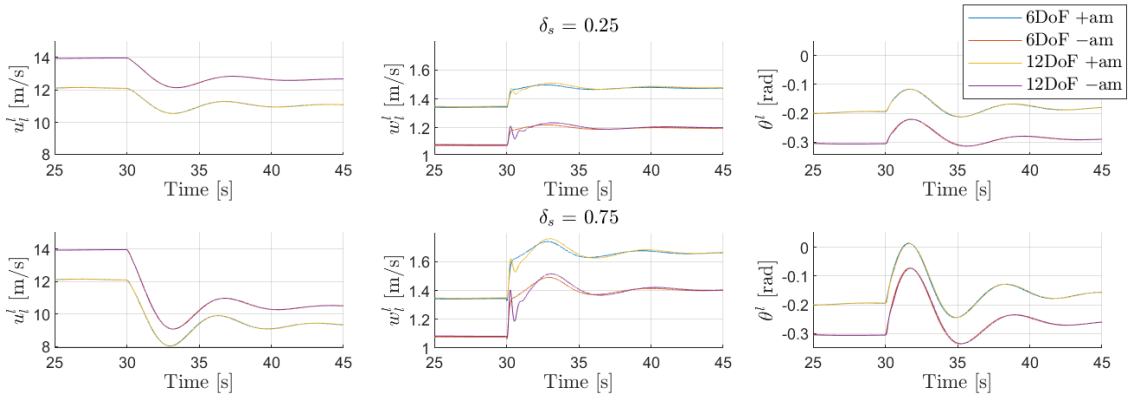

Figure 14: Dynamic response δ_s

The same analysis can be made for an asymmetric deflection. The control deflection is changed from zero deflection to a constant asymmetric deflection of 0.25 and 0.75. The dynamic response of the flight behavior is shown in 15-17. The exact characteristics of the response are given in Table 2. Here the apparent mass also adds a steady state offset to the system, in the forward and downward velocity as well as in the angle θ^{l}. A steady state in the flight dynamics is introduced in the side velocity, the angular velocities and the roll angle. They all start from zero and converge to a constant value. Differences between the 6 DoF and 12 DoF model are visible. The 12 DoF model shows oscillations in $v_{\mathrm{l}}^{\mathrm{l}}$, $r_{\mathrm{l}}^{\mathrm{l}}$ and some minor oscillations in $p_{\mathrm{l}}^{\mathrm{l}}$.

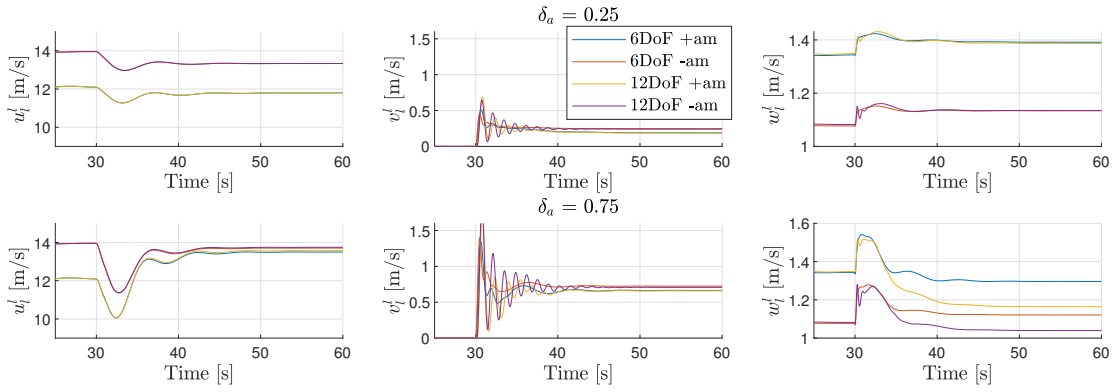

Figure 15: Dynamic response $\delta_a \rightarrow \vec{V}_{\mathrm{l}}^{\mathrm{l}}$

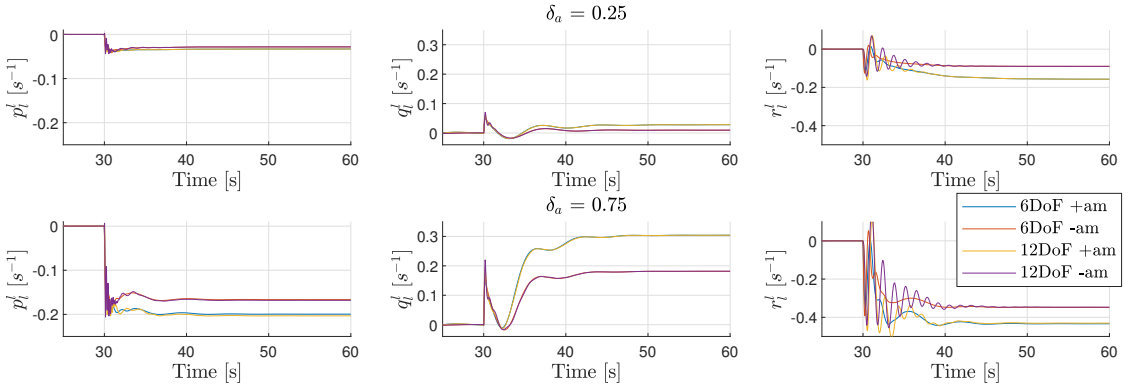

Figure 16: Dynamic response $\delta_a \rightarrow \vec{\omega}_1^1$

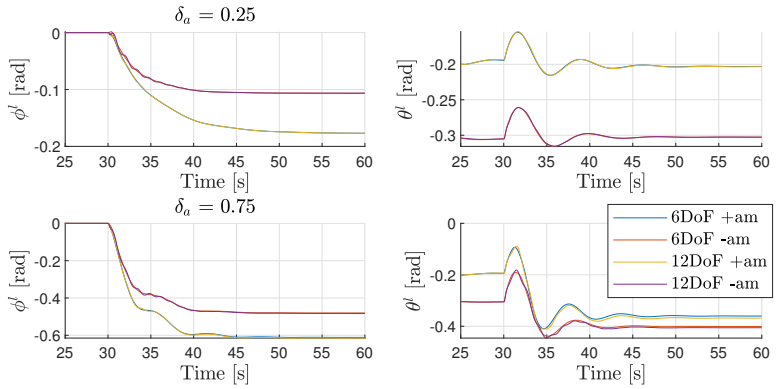

Figure 17: Dynamic response $\delta_a \rightarrow \vec{\eta}^1$

Table 2: Dynamic behavior for an asymmetric input

		$\delta_a = 0.25$			$\delta_a = 0.75$		
Variable	**Model**	t_r [s]	t_s [s]	M_p [-]	t_r [s]	t_s [s]	M_p [-]
u_1^1	6DoF	0.76	12.88	1.70	6.31	11.03	2.467
	12DoF	0.67	13.03	1.81	6.41	11.11	2.38
v_1^1	6DoF	0.16	9.87	1.72	0.19	4.00	1.02
	12DoF	0.16	9.87	2.73	0.18	6.92	1.66
w_1^1	6DoF	0.17	11.29	1.01	9.81	14.12	5.33
	12DoF	0.09	12.86	1.16	6.65	10.80	1.93
p_1^1	6DoF	0.15	1.87	1.00	0.29	1.05	1.00
	12DoF	0.05	2.06	1.08	0.26	1.51	1.02
q_1^1	6DoF	0.05	13.02	1.68	9.78	9.80	1.04
	12DoF	0.05	13.10	1.61	9.86	9.92	1.04
r_1^1	6DoF	10.32	10.34	1.09	2.57	6.79	1.00
	12DoF	0.28	10.43	1.45	0.26	7.26	1.30

5 Linearization

Both the 6 DoF and 12 DoF models, which are developed in this report are nonlinear. To still get an intuitive understanding on how the non-linearities affect the model, the model is linearized around an equilibrium point. The linearizations are compared with each other to assess how different the model behavior in these equilibrium points actually is. A comparison is made through the frequency responses of the different linearizations. The model is linearized through a first order Taylor expansion. The general expression of a non-linear state space model is as follows

$$\begin{aligned} \dot{x} &= f(x, u, w), \\ y &= h(x). \end{aligned} \tag{55}$$

A first order Taylor approximation is made in the equilibrium point (x^*, u^*, w^*) leading to the expression

$$\dot{x} \approx f(x^*, u^*, w^*) + \underbrace{\left.\frac{\partial f(x,u,w)}{\partial x}\right|_{x^*,u^*,w^*}}_{A}(x - x^*) + \underbrace{\left.\frac{\partial f(x,u,w)}{\partial u}\right|_{x^*,u^*,w^*}}_{B}(u - u^*) + \underbrace{\left.\frac{\partial f(x,u,w)}{\partial w}\right|_{x^*,u^*,w^*}}_{W}(w - w^*) \tag{56}$$

and

$$y \approx h(x^*) + \underbrace{\left.\frac{\partial h(x)}{\partial x}\right|_{x^*}}_{C}(x - x^*). \tag{57}$$

When considering a wind disturbance, the model leads to an equilibrium point for constant symmetric deflections. For constant asymmetric deflection the model does not lead to a equilibrium point. As a result the term $f(x^*, u^*, w^*)$ is not zero. This term is seen as a constant input, by introducing ν as an auxiliary input. By expressing the system variables $(x - x^*)$ as $\tilde{x}$, $(u - u^*)$ as $\tilde{u}$, $(w - w^*)$ as $\tilde{w}$ and $y - h(x^*)$ as $\tilde{y}$ the linearized system is described as

$$\begin{aligned} \dot{\tilde{x}} &\approx A\tilde{x} + \nu + W\tilde{w} \\ \tilde{y} &\approx C\tilde{x}. \end{aligned} \tag{58}$$

here, ν is expressed as

$$\nu = B\tilde{u} + f(x^*, u^*, w^*) \tag{59}$$

Since the point (x^*, u^*, w^*) is not necessarily an equilibrium point of the system, the system is linearized along an equilibrium trajectory. The system is linearized in all the points in the trajectory. All these models together result in a linear parameter varying (LPV) model. An LPV model varies over the scheduling variable p. The the scheduling variable $p(t)$ may vary over time and is assumed to be exogenous. This results in a LPV system as

$$\begin{aligned} \dot{\tilde{x}} &\approx A(p)\tilde{x} + \nu(\tilde{u}, p) + W(p)\tilde{w} \\ \tilde{y} &\approx C(p)\tilde{x}. \end{aligned} \tag{60}$$

with p related to the equilibrium trajectory as

$$p = \Psi(x^*, u^*, w^*) \tag{61}$$

In this report a linearization is made for zero wind disturbance. For a constant input, the states

of the model converge to an equilibrium position. The model can be linearized in this equilibrium point and one linear system is obtained for each constant input. Not all the states converge to an equilibrium point. In the 6 DoF model this are the position vectors and the yaw angle. The derivative of the yaw angle becomes constant and can be embedded as a constant input to the system. This is also done in (59). The position does not affect the input-output relation and can be taken out of the linearized model.

The position vectors and the yaw angles do not converge to an equilibrium point in the 12 DoF model. This is problematic since the dynamics depend on these states. The tension force is dependent on the positions and the yaw angles. This can be solved by recognizing that the model is only dependent on the relative position ($\vec{r}_{\mathrm{t}}^{\,\mathrm{p}}$) and the relative yaw angle ($\psi^{\,\mathrm{t}}$), expressed in the parafoil frame. These state actually do converge to an equilibrium point and can be determined based on other converging state variables as

$$\begin{bmatrix} \dot{\vec{r}}_{\mathrm{t}}^{\,\mathrm{p}} \\ \dot{\vec{\eta}}^{\,\mathrm{t}} \end{bmatrix} = \underbrace{\begin{bmatrix} I^{3\mathrm{x}3} & -R(\vec{\eta}^{\,\mathrm{t}}) & [\vec{r}_{\mathrm{t}}^{\,\mathrm{p}}]_{\times} & 0 \\ 0 & 0 & T(\phi^{\mathrm{p}}, \theta^{\mathrm{p}}) & -T(\phi^{\mathrm{l}}, \theta^{\mathrm{l}}) \end{bmatrix}}_{E} \zeta. \tag{62}$$

Here $[\vec{r}_{\mathrm{t}}^{\,\mathrm{p}}]_{\times}$ is the crossproduct matrix of $\vec{r}_{\mathrm{t}}^{\,\mathrm{p}}$. By adding these variables to state vector as x_3, the state equation is rewritten as

$$\dot{x} = \begin{bmatrix} 0 & J(x_1) & 0 \\ 0 & M^{-1}[C_{\zeta}(x_2) + D_{\zeta}(x_3)] & M^{-1}C_{\xi}(x_3) \\ 0 & E(x_1, x_3) & 0 \end{bmatrix} x + \begin{bmatrix} 0 \\ M^{-1}\left[D(x_2, u) + G(x_1) + S\right] \\ 0 \end{bmatrix}. \tag{63}$$

Now the actual position of the parafoil and the load do not contribute to the systems dynamics and also not to the input-output relation. The same hold for the parafoil yaw angle. The load yaw angle does not contribute to the systems dynamics, but is an output. The yaw rate converges to an equilibrium point, which can be treated as an additional constant input.

The system is linearized for different symmetric deflection (δ_s) and asymmetric deflections (δ_a), which leads to different steady state point x^* and u^*. The wind disturbance is kept at zero. For each linearization the transfer function is constructed from the input $\tilde{u}$ to the output y. Figure 18 and 19 show the resulting frequency responses for the 6 DoF model.

The responses of the 6 DoF model show two interesting things. First, the low frequency behavior differs per linearization. Especially the low frequency gain for the zero deflection linearization differs. Secondly, the resonances and the anti-resonances are placed at varying frequencies per linearization. The different resonances and anti-resonances also result in different phases. The left and right deflection are 180 [deg] shifted for linearizations at a constant symmetric deflection.

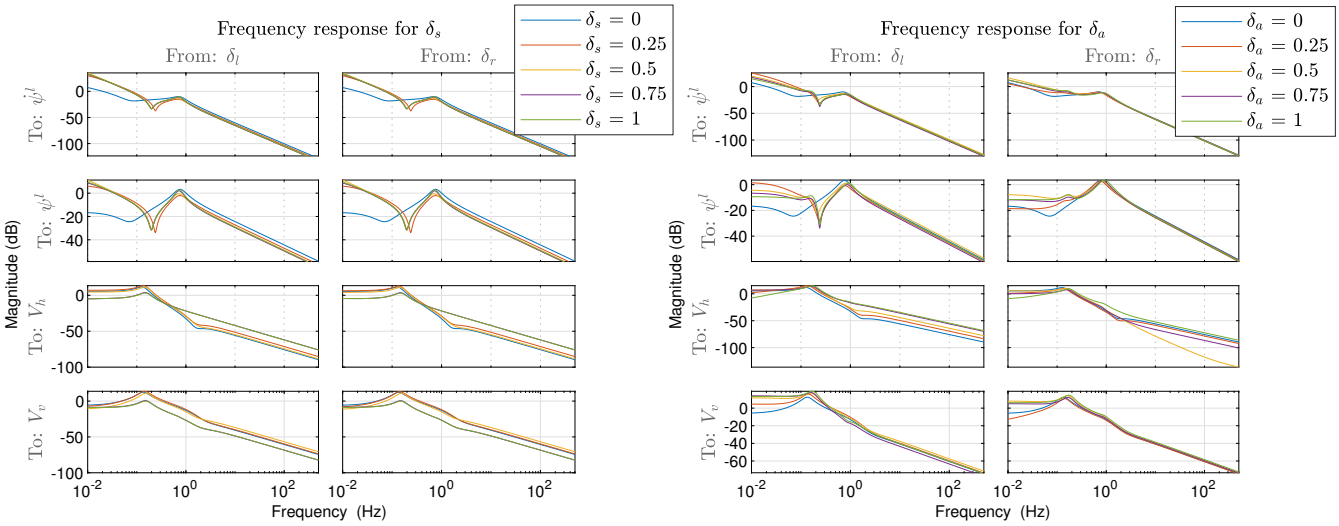

Figure 18: Magnitude response linear 6 DoF models

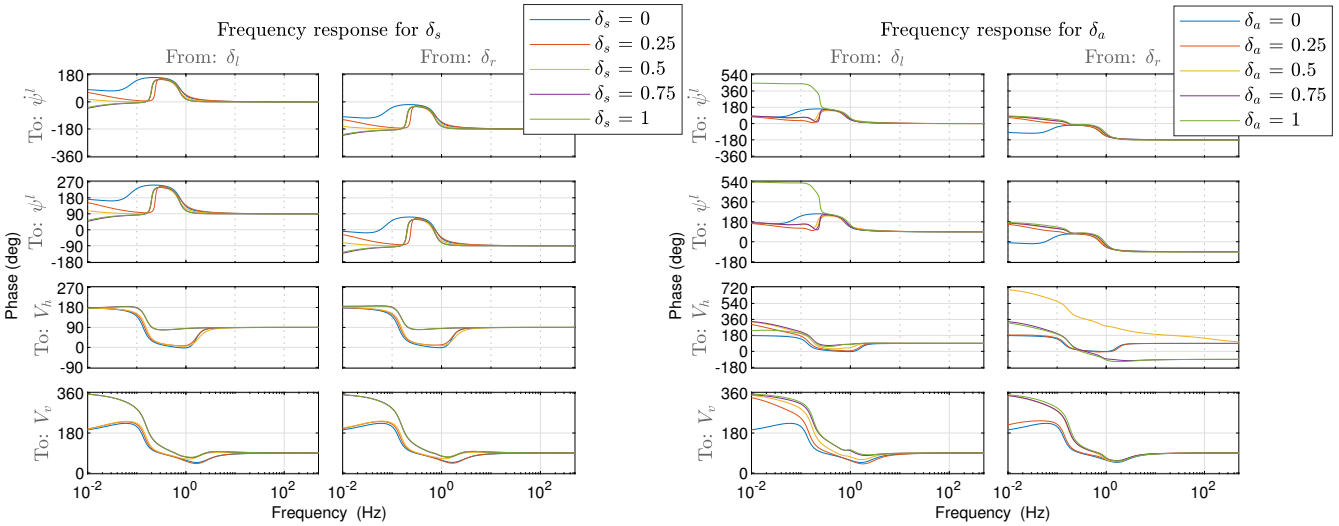

Figure 19: Phase response linear 6 DoF models

The resulting linearizations for the 12 DoF model is shown in Figure 20 and 21. The overall system behavior is similar to the 6 DoF model, with different low frequency gains and moving resonances and anti-resonances. The linearizations show that the 12 DoF model has additional behavior in terms of resonances and anti resonances, which vary for the different equilibrium point. Especially the response of $V_{\mathrm{h}}^{\mathrm{n}}$ gives changing behavior for a linearization in an asymmetric deflection point. The phase changes for different linearizations.

The 6 DoF and 12 DoF models are linearized in different equilibrium points. The resulting models have varying linear behavior in each equilibrium point. In the magnitude responses the

low frequency gains are different and the positions of the resonances and anti-resonances differ.

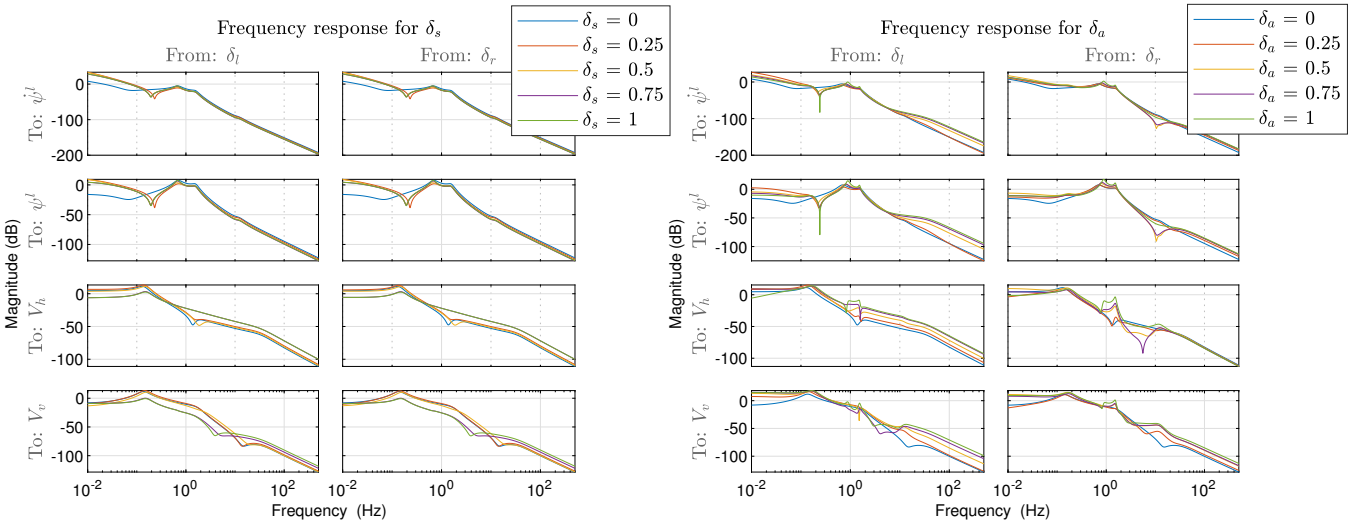

Figure 20: Magnitude response linear 12 DoF models

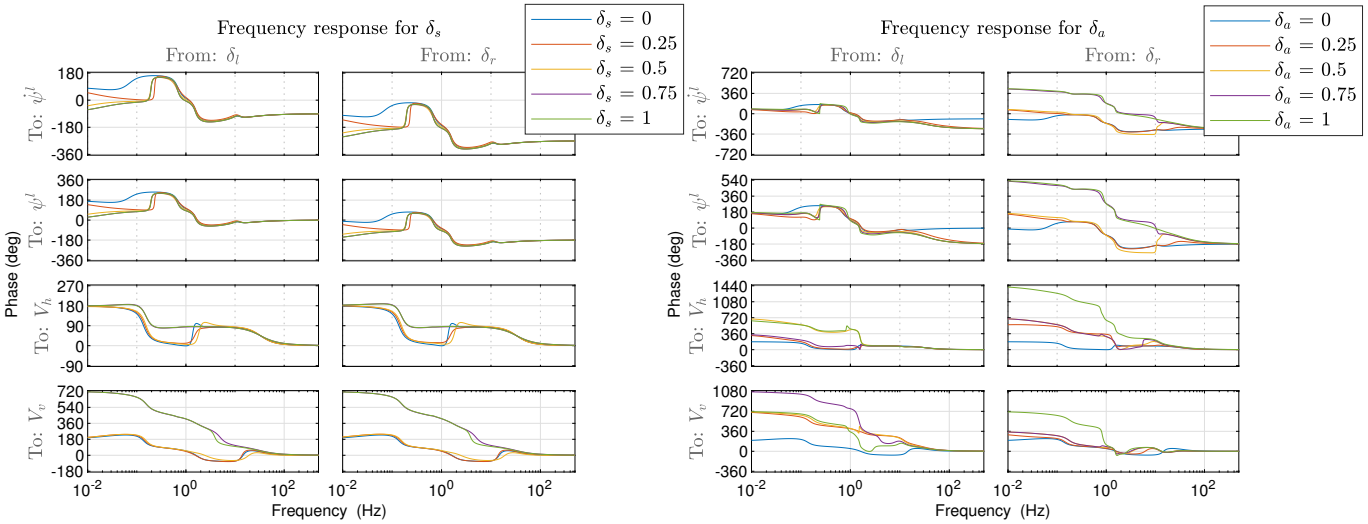

Figure 21: Phase response linear 12 DoF models

6 Validation

The constructed models are validated w.r.t. the simulation results shown by Van der Kolf in [21]. This paper presents a complete set of parameters together with the simulation results. Van der Kolf simulates an 8 DoF model. The paper presents the following variables for the system, with which the models can be validated:

- The angle of attack of the parafoil (α_{p}),
- The parafoil pitch angle (θ_{p}),
- The load glide path angle (γ_{l}),
- The horizontal velocity of the load ($V_{\mathrm{h}}^{\mathrm{n}}$),
- The vertical velocity of the load ($V_{\mathrm{v}}^{\mathrm{n}}$),

In [10] the corresponding 8 DoF model is presented. The load is able to rotate relative to the parafoil with a pitch and yaw angle. Some differences between the models are expected due to the different model order. Moreover, the model used, do not include the apparent mass. The added behavior to the flight dynamics is already discussed. therefore, the validation will be done without the apparent mass effect. First the steady state flight behavior, resulting from a constant symmetric deflection is compared. The symmetric deflections varies from 0 to 1 [-]. Next the steady state flight behavior, as a result of an asymmetric deflection, is compared. The asymmetric deflection varies between 0 and 1 [-]. Lastly, both the dynamic flight behavior as a result of an symmetric deflection and an asymmetric deflection are compared to the reported simulations of Van der Kolf.

6.1 Steady state flight behavior

The horizontal load velocity is calculated as

$$V_{\mathrm{h}}^{\mathrm{n}} = \sqrt{(u_{\mathrm{l}}^{\mathrm{n}})^2 + (v_{\mathrm{l}}^{\mathrm{n}})^2} \tag{64}$$

The vertical velocity equals the $w_{\mathrm{l}}^{\mathrm{n}}$ and the glide path angle can be determined as

$$\gamma^{\,\mathrm{l}} = \tan^{-1}\left(\frac{V_{\mathrm{v}}^{\mathrm{n}}}{V_{\mathrm{h}}^{\mathrm{n}}}\right) \tag{65}$$

Table 3: Difference in steady state behavior

Variable	Van der Kolf	6DoF model	12DoF model
$V_{\mathrm{h}}^{\mathrm{n}}$ [m/s]	12.99	12.98	12.98
$V_{\mathrm{v}}^{\mathrm{n}}$ [m/s]	5.14	5.22	5.22
$\gamma^{\,\mathrm{l}}$ [deg]	21.63	21.91	21.91
α^{p} [deg]	3.53	3.53	3.53
θ^{p} [deg]	-18.1	-18.39	-18.37

Table 3 shows the steady state behavior for zero control deflection, together with the reported values of Van der Kolf. There are only small differences. $V_{\mathrm{v}}^{\mathrm{n}}$ has a difference of 0.08 [m/s], resulting in 0.28 [deg] difference in $\gamma^{\,\mathrm{l}}$. The parafoil pitch angle (θ^{p}) differs with 0.28 [deg]. The

steady state flight behavior, as a result of an constant symmetric deflection, of the 6DoF and 12Dof model with the reported values are shown in Figure 22. The found steady state values are almost the same for zero deflection but diverge for increasing symmetric deflections. For a symmetric deflection of 1 the 6DoF and the 12DoF model show as sudden increase w.r.t. to the lower deflections. This is not the case in the presented simulation results of Van der Kolf.

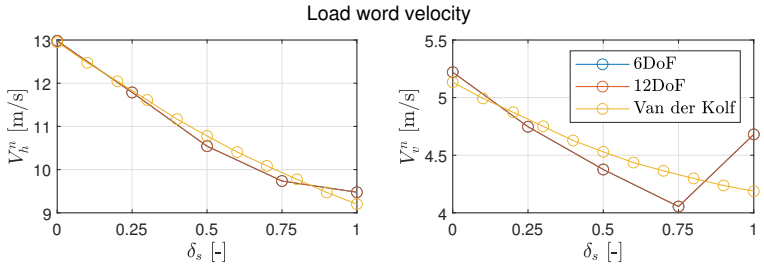

Figure 22: Steady state response to δ_s

The steady state response, resulting from constant asymmetric deflections are shown in Figure 23. The steady states is the same for zero deflection, but diverge for increasing asymmetric deflections. The horizontal velocity stays between 13 and 12.4 [m/s] for both models, while the reported velocity increases first to 14.4 [m/s] and decreases for asymmetric deflections higher than 0.7 [-] to 12.5 [m/s]. The maximum difference is 1.9 [m/s]. The vertical velocity are both increasing. The modeled velocity increases slower than the reported, leading to a difference of maximal 7 [m/s]. The yaw rate gives a maximum difference of 0.2 [rad/s]. The absolute differences are shown in Table 4. The difference in turning rate is not given for symmetric deflections. The system is not turning for a symmetric deflection and therefore it is also not reported by Van der Kolf.

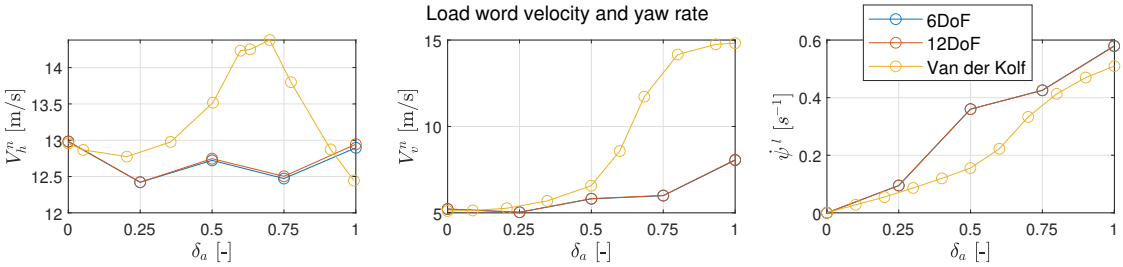

Figure 23: Steady state response to δ_a

Table 4: Difference in steady state behavior

Variable	Model	δ_s				δ_a			
		0.25 [-]	0.5 [-]	0.75 [-]	1 [-]	0.25 [-]	0.5 [-]	0.75 [-]	1 [-]
Diff. V_h^n [m/s]	6DoF	0.04	0.24	0.19	0.27	0.42	0.78	1.52	0.49
	12DoF	0.04	0.24	0.19	0.27	0.41	0.76	1.49	0.53
Diff. V_v^h [m/s]	6DoF	0.07	0.15	0.28	0.49	0.36	0.78	7.11	6.77
	12DoF	0.07	0.15	0.28	0.49	0.36	0.77	7.10	6.74
Diff. $\dot{\psi}^l$ [rad/s]	6DoF					0.02	0.20	0.05	0.07
	12DoF					0.02	0.20	0.05	0.07

6.2 Dynamical flight behavior

The same model variables are used to compare the dynamic flight behavior as was used for the steady states flight behavior. For the response to a symmetric deflection, the horizontal and vertical velocity of the load are shown. For an asymmetric deflection the horizontal and vertical velocity of the load and yaw rate are presented. The dynamic flight behavior of the models is shown in Figure 24. The deflection is changed from a constant zero deflection to a constant symmetric deflection of 1. It is already shown that the steady state values differ, but the intermediate dynamic flight behavior looks similar for all models. In general the oscillation frequency of the reported values is slightly higher. The reported values show a bit less damping resulting in a longer settling time. The differences in rise time, settling time and overshoot are given in Table 5. This table also shows a large difference in relative overshoot in the vertical load velocity. The 6 DoF and 12 DoF make a relative smaller step compared to reported simulation.

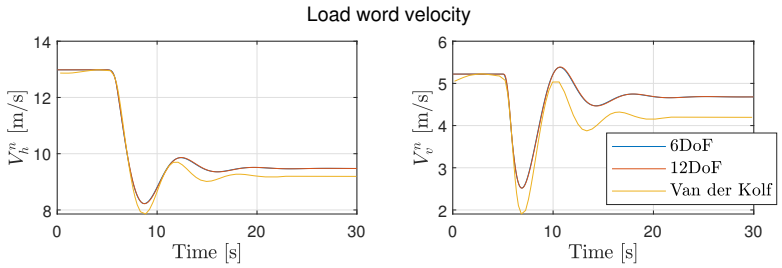

Figure 24: Velocity response from $\delta_s = 0$ to $\delta_s = 1$

The dynamic response of both models resulting from an asymmetric deflection is shown in Figure 25. The input is changed from zero deflection to 0.4 [-] asymmetric deflection. The steady state flight behavior is different. The result is inline with the steady state response of Figure 23. The dynamic flight behavior of the horizontal and vertical velocity of the 6 DoF and 12 DoF model is similar to the reported dynamic flight behavior. Table 5 shows the difference in rise time settling time and relative overshoot. The large differences are a result of the different steady states values. The step the 6 DoF and 12 DoF models are making from the steady state at 0 [s] to the steady state at 30 [s] is much smaller than the step taken by the reported velocity. The smaller step result in different rise time, settling time and overshoot. The yaw rate shows other dynamics, than the reported yaw rate. The oscillation in the yaw rate is a result of the tension line model constraining the relative movement between the parafoil and the load. The 6 DoF

does not show any oscillation, since there is no relative movement. The oscillation of the 12 DoF model are more damped than the oscillations in the reported yaw rate.

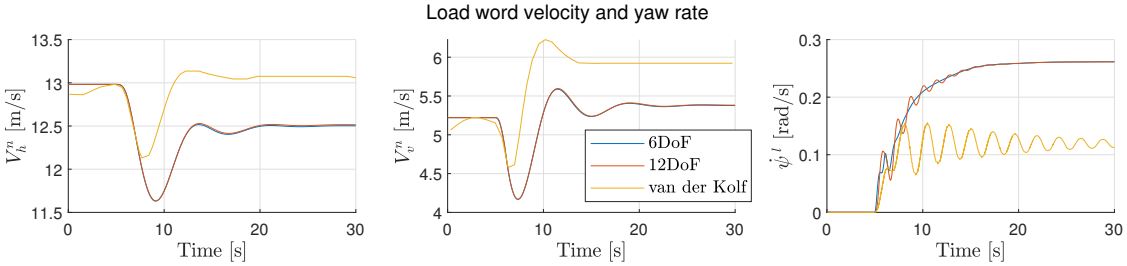

Figure 25: Dynamic response to δ_s

Table 5: Difference in Dynamic behavior

Variable	**Model**	δ_s			δ_a		
		diff. t_r [s]	diff. t_s [s]	diff. M_p [-]	diff. t_r [s]	diff. t_s [s]	diff. M_p [s]
V_h^n [m/s]	6DoF	0.03	0.74	0.03	5.60	4.96	3.00
	12DoF	0.05	0.83	0.03	5.59	6.56	2.93
V_v^h [m/s]	6DoF	0.05	2.03	1.31	3.55	8.50	6.19
	12DoF	0.02	2.18	1.32	3.54	7.14	5.96
$\dot{\psi}^l$ [rad/s]	6DoF				3.69	1.16	0.56
	12DoF				3.34	0.95	0.56

7 Discussion and Conclusion

Some remarks should be made on the presented work. First of all, Yakimenko argues in [4] that one of the important parts of the aerodynamic drag in a PADS is the line drag. This is not discussed in this report, but could be easily taken into account in the sum of forces and moments in the EoM of the parafoil and the load.

The simulation parameters used in Sec. 4 are also the parameter set given by Van der Kolf in [21]. This set is extensive, but does not include average parafoil thickness and the arc angle of the parafoil. These are needed to determine the apparent mass and inertia matrices. Therefore these parameters are estimated. How accurate these estimations are and how they influence the overall apparent mass effect is not analyzed. Next, Yakimenko argues in [4], that the term $\vec{V}^{\mathrm{p}}_{\mathrm{p,air}} \times m^{\mathrm{p}}_{\mathrm{p_m}} \vec{V}^{\mathrm{p}}_{\mathrm{p,air}}$ can be neglected in the apparent mass effect, since it could be included in the aerodynamic expressions. It remains unclear when this is the case or when not. The term $\vec{V}^{\mathrm{p}}_{\mathrm{p,air}} \times m^{\mathrm{p}}_{\mathrm{p_m}} \vec{V}^{\mathrm{p}}_{\mathrm{p,air}}$ is the main contribution in the steady state offset due to the apparent mass in Sec 4. For instance consider the system in steady state for a constant symmetric deflection input. The angular velocity, acceleration and angular acceleration are zero. This simplifies the apparent mass effect to only $\vec{V}^{\mathrm{p}}_{\mathrm{p,air}} \times m^{\mathrm{p}}_{\mathrm{p_m}} \vec{V}^{\mathrm{p}}_{\mathrm{p,air}}$, resulting in the steady state offsets given in Figure 8.

A note can be made on the model comparison in the validation. The steady state behavior of the model is in essence a force moment balance of the aerodynamic effect, the gravity and the apparent mass. Therefore, the steady state is highly dependent on the accuracy of the aerodynamic force and moment. In this research the aerodynamics presented in [21] is used, in which already some numerical mistakes are found in the presented matrices. Next to this the presented model uses a nonlinear expression to constrain the relative yaw between the parafoil and the load. The 12 DoF uses a linear spring-damper system. These two things together with the difference in model order, most likely result in the differences present in the validation. The validation shows that the model has the same behavior as the reported model for zero deflection. Similar flight behavior is shown for symmetric deflections. The steady state behavior diverges with maximal 0.4 [m/s]. For asymmetric deflections the steady state behavior is different. The dynamic flight behavior is similar in the velocity, but the dynamic flight behavior is different in the yaw rate.

In the future this research can be extended by weakening the rigid body assumption of the parafoil and dividing it in multiple panels. The panels can rotate with respect to each other. This is briefly explained in Sec. 3.7 and an expression for the aerodynamic force per panel is presented there. Furthermore, a tension line representation could be extended towards modeling real tension lines, in a realistic configuration. The tension moments could then also be modeled as a result of the tension force. This is also briefly discussed in Sec. 3.7.

To conclude on the research question: "Which dynamic effects acting on the SR during the terminal guidance phase should be considered, to describe the flight dynamics of the Space Rider w.r.t. the desired landing precision and landing constraints of the GNC system? The literature review gives an expectation". The 6 DoF model describes the overall flight dynamics based on the aerodynamics, gravity and the apparent mass. The 12 DoF model adds internal dynamics due to relative motion between the load and the parafoil. The following effect are considered relevant in the literature. The gravity, aerodynamics and the apparent mass. The results of the constructed models, show that The 6 DoF model describes indeed the overall flight dynamics. The steady state flight behavior of the 6 DoF model is similar to the steady state flight behavior

of the 12 DoF. Small differences are visible, when in the 12 DoF model, the load is rotated relative to the parafoil. The 12 DoF model adds oscillations to the dynamic behavior, due to the spring-damper system used for the tension line. This is also visible in the linearization. The frequency responses of the 6 DoF and the 12 DoF models are similar, but the response of the 12 DoF model shows additional dynamics. The gravity and the aerodynamics act similar in both models. The model is simulated with and without the apparent mass effect. Comparing the results shows, that the gravity and aerodynamics account for most of the flight dynamics. The apparent mass adds a steady state offset in the flight behavior.

The question remains how relevant this is to the SR terminal guidance phase. The gravity, aerodynamics and apparent mass influence the flight behavior, such that is would be important to include the dynamic effects for position, velocity or heading control. In terms of position, velocity or heading, the 12 DoF does not add any flight behavior, compared to the 6 DoF model. The 12DoF model adds dynamics behavior, which is relevant for a changing wind disturbance, or during the landing. The 12 DoF model could show how the load is oscillating w.r.t. the parafoil during a landing. This influences the impact of the landing.

In the future, the model developed in this report can be used to improve the GNC of the Space Rider during the terminal descent phase. The constructed model and the LPV description of the model along an equilibrium trajectory, give a first impressions for a control strategy. The linearizations show that the nonlinear model has moving resonances and varying low frequency gains. Therefore, it is expected that a nonlinear controller will results in a higher GNC performance, instead of a linear controller. With the constructed LPV model an LPV type of controller can be used for the GNC solution.

References

[1] S. Aerospace, C. Severo, O. Ptm, T. Cantos, D. S. S. L. U, R. D. Poniente, and T. Cantos, "The Design of the GNC of the Re-entry Module of Space," *8th European Conference for Aeronautics and Space Sciences*, 2019.

[2] A. Figueroa-González, F. Cacciatore, and R. Haya-Ramos, "Landing guidance strategy of space rider," *Journal of Spacecraft and Rockets*, vol. 58, no. 4, pp. 1220–1231, 2021.

[3] O. A. Yakimenko, "On the development of a scalable 8-DoF model for a generic parafoil-payload delivery system," in *Collection of Technical Papers - 18th AIAA Aerodynamic Decelerator Systems Technology Conference and Seminar*, no. January, pp. 642–654, 2005.

[4] O. A. Yakimenko, *Precision Aerial Delivery Systems: Modeling, Dynamics, and Control*. 2015.

[5] G. Bonaccorsi, *Guidance & Control of a Parafoil-Based Landing on Titan*. PhD thesis, 2019.

[6] B. J. Rademacher, P. Lu, A. L. Strahan, and C. J. Cerimele, "In-flight trajectory planning and guidance for autonomous parafoils," *Journal of Guidance, Control, and Dynamics*, vol. 32, no. 6, pp. 1697–1712, 2009.

[7] M. Ward, M. Costello, and N. Slegers, "Specialized system identification for autonomous parafoil and payload systems," in *AIAA Atmospheric Flight Mechanics Conference 2010*, 2010.

[8] E. Mooij, R. Mazouz, and M. B. Quadrelli, "Convex optimization guidance for precision landing on titan," in *AIAA Scitech 2021 Forum*, pp. 1–21, 2021.

[9] M. Ward, S. Culpepper, and M. Costello, "Parafoil control using payload weight shift," *Journal of Aircraft*, vol. 51, no. 1, pp. 204–215, 2014.

[10] C. Redelinghuys, "A flight simulation algorithm for a parafoil suspending an air vehicle," *Journal of Guidance, Control, and Dynamics*, vol. 30, no. 3, pp. 791–803, 2007.

[11] N. J. Slegers, "Effects of canopy-payload relative motion on control of autonomous parafoils," in *Journal of Guidance, Control, and Dynamics*, vol. 33, pp. 116–125, 2010.

[12] E. Zhu, Q. Sun, P. Tan, Z. Chen, X. Kang, and Y. He, "Modeling of powered parafoil based on Kirchhoff motion equation," *Nonlinear Dynamics*, vol. 79, no. 1, pp. 617–629, 2015.

[13] Niccolò GLOUCHTCHENKO, "Multibody parafoil-payload model for SpaceRider trajectory and inflation loads analysis," p. 111, 2018.

[14] P. B. Lissaman and G. J. Brown, "Apparent Mass effects on parafoil dynamics," in *AIAA/AHS/ASEE Aerospace Design Conference, 1993*, 1993.

[15] T. M. Barrows, "Apparent mass of parafoils with spanwise camber," in *16th AIAA Aerodynamic Decelerator Systems Technology Conference and Seminar*, vol. 39, 2001.

[16] T. Jann, "Aerodynamic coefficients for a parafoil wing with arc anhedral - Theoretical and experimental results," in *17th AIAA Aerodynamic Decelerator Systems Technology Conference and Seminar*, no. May, 2003.

[17] J. S. Lingard, "Ram-Air Parachute Design," *Precision Aerial Delivery Seminar, 13th AIAA Aerodynamic Decelerator Systems Technology Conference*, no. May, pp. 1–51, 1995.

[18] T. Bennett and R. Fox, *Design, Development & Flight Testing of the NASA X-38 7500 ft2 Parafoil Recovery System*.

[19] S. Müller, M. Heise, O. Wagner, and G. Sachs, "Paralabs an integrated design tool for parafoil systems," in *Collection of Technical Papers - 18th AIAA Aerodynamic Decelerator Systems Technology Conference and Seminar*, pp. 704–714, 2005.

[20] N. Slegers, E. Beyer, and M. Costello, "Use of variable incidence angle for glide slope control of autonomous parafoils," in *Journal of Guidance, Control, and Dynamics*, vol. 31, pp. 585–596, 2008.

[21] G. Van Der Kolf, "Flight Control System for an Autonomous Parafoil," no. December, 2013.

[22] D. Bodmer, M. Krenmayr, and F. Holzapfel, "Asymptotic tracking position control with active oscillation damping of a multibody Mars vehicle using two artificial augmentation approaches," *CEAS Space Journal*, no. 0123456789, 2021.

[23] M. Ben-Ari, "A Tutorial on Euler Angles and Quaternions," tech. rep., Weizmann Institute of Science, 2014. AVALAIBLE AT `https://www.weizmann.ac.il/sci-tea/benari/sites/sci-tea.benari/files/uploads/softwareAndLearningMaterials/quaternion-tutorial-2-0-1.pdf`.

[24] J. LINGARD, "The Aerodynamics of Gliding Parachutes," 1986.